Cell Reports

Article

Arginine catabolism is essential to polymyxin dependence in *Acinetobacter baumannii*

Graphical abstract

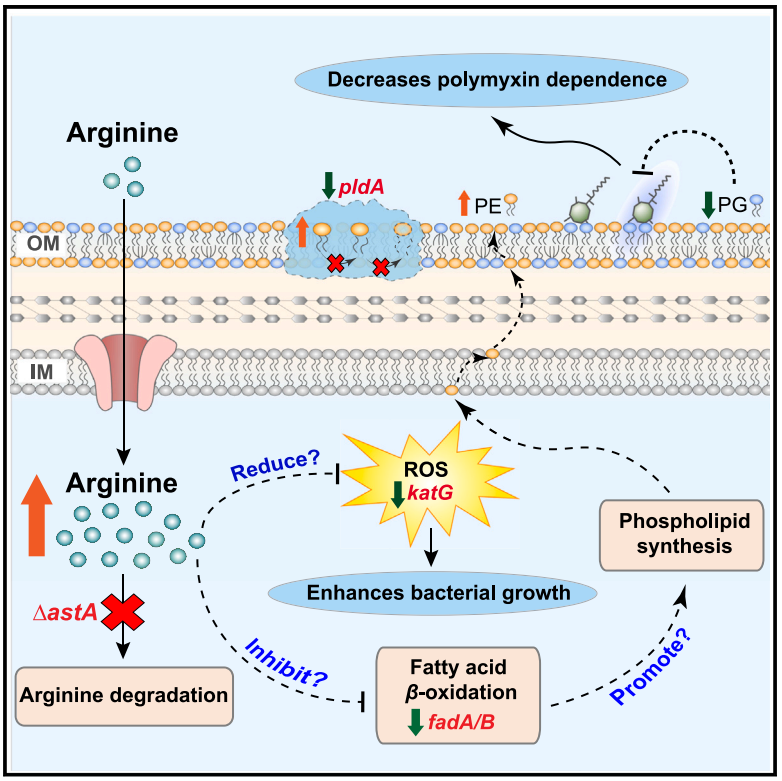

Highlights

- Arginine supplementation enhances the detection of polymyxin-dependent *A. baumannii*
- Critical genes and metabolites in arginine catabolism were significantly affected
- *ΔastA* perturbs membrane lipid composition, reducing interaction with polymyxins

Authors

Mei-Ling Han, Yasser Alsaadi, Jinxin Zhao, ..., Darren J. Creek, Tony Velkov, Jian Li

Correspondence

meiling.han@monash.edu (M.-L.H.), jian.li@monash.edu (J.L.)

In brief

Polymyxin-dependent *Acinetobacter baumannii* is highly resistant to the last-line polymyxins and often escapes detection in clinical microbiology diagnostic laboratories. Han et al. discovered the critical role of arginine in enhancing bacterial detection, demonstrating how arginine metabolism alters the membrane composition in polymyxin-dependent bacteria, thereby reducing interactions with polymyxins.

Han et al., 2024, Cell Reports *43*, 114410
July 23, 2024
https://doi.org/10.1016/j.celrep.2024.114410

CellPress

Cell Reports

CellPress
OPEN ACCESS

Article

Arginine catabolism is essential to polymyxin dependence in *Acinetobacter baumannii*

Mei-Ling Han,[1,2,9,*] Yasser Alsaadi,[1,2] Jinxin Zhao,[1,2] Yan Zhu,[1,2] Jing Lu,[1,2] Xukai Jiang,[3] Wendong Ma,[1,2] Nitin A. Patil,[1,2] Rhys A. Dunstan,[1,2] Anton P. Le Brun,[4] Hasini Wickremasinghe,[1,2] Xiaohan Hu,[1,2] Yimin Wu,[1,2] Heidi H. Yu,[1,2] Jiping Wang,[1,2] Christopher K. Barlow,[5] Phillip J. Bergen,[1,2] Hsin-Hui Shen,[6] Trevor Lithgow,[1,2] Darren J. Creek,[5,7] Tony Velkov,[8] and Jian Li[1,2,*]

[1]Infection Program and Department of Microbiology, Biomedicine Discovery Institute, Monash University, Clayton, VIC 3800, Australia
[2]Centre to Impact AMR, Monash University, Clayton, VIC 3800, Australia
[3]National Glycoengineering Research Centre, Shandong University, Qingdao 266237, China
[4]Australian Centre for Neutron Scattering, Australian Nuclear Science and Technology Organisation, Locked Bag 2001, Kirrawee DC, NSW 2232, Australia
[5]Monash Proteomics and Metabolomics Facility, Biomedicine Discovery Institute, Monash University, Clayton, VIC 3800, Australia
[6]Department of Materials Science and Engineering, Faculty of Engineering, Monash University, Clayton, VIC 3800, Australia
[7]Drug Delivery, Disposition and Dynamics, Monash Institute of Pharmaceutical Sciences, Monash University, 381 Royal Parade, Parkville, VIC 3052, Australia
[8]Department of Pharmacology, Biomedicine Discovery Institute, Monash University, Clayton, VIC 3800, Australia
[9]Lead contact
*Correspondence: meiling.han@monash.edu (M.-L.H.), jian.li@monash.edu (J.L.)
https://doi.org/10.1016/j.celrep.2024.114410

SUMMARY

Polymyxins are often the only effective antibiotics against the "Critical" pathogen *Acinetobacter baumannii*. Worryingly, highly polymyxin-resistant *A. baumannii* displaying dependence on polymyxins has emerged in the clinic, leading to diagnosis and treatment failures. Here, we report that arginine metabolism is essential for polymyxin-dependent *A. baumannii*. Specifically, the arginine degradation pathway was significantly altered in polymyxin-dependent strains compared to wild-type strains, with critical metabolites (e.g., L-arginine and L-glutamate) severely depleted and expression of the *astABCDE* operon significantly increased. Supplementation of arginine increased bacterial metabolic activity and suppressed polymyxin dependence. Deletion of *astA*, the first gene in the arginine degradation pathway, decreased phosphatidylglycerol and increased phosphatidylethanolamine levels in the outer membrane, thereby reducing the interaction with polymyxins. This study elucidates the molecular mechanism by which arginine metabolism impacts polymyxin dependence in *A. baumannii*, underscoring its critical role in improving diagnosis and treatment of life-threatening infections caused by "undetectable" polymyxin-dependent *A. baumannii*.

INTRODUCTION

Multidrug-resistant (MDR) *Acinetobacter baumannii* is one of the most common causative pathogens of nosocomial infections such as pneumonia, sepsis, and meningitis.[1,2] The World Health Organization has designated carbapenem-resistant *A. baumannii* one of the three top-priority pathogens (Priority 1: Critical) urgently requiring the discovery and development of novel antibiotics.[3] Given their significant activity against many gram-negative bacteria, polymyxin B and colistin (also known as polymyxin E) are increasingly used as a last-line therapy for infections caused by problematic pathogens, including MDR *A. baumannii*.[4–6]

Polymyxins are cationic lipopeptides that specifically bind to the lipid A moiety of lipopolysaccharide (LPS) in the outer membrane of gram-negative bacteria.[7] The initial interaction between the positively charged polymyxin molecule and negatively charged lipid A is essential for the antimicrobial activity. However, gram-negative bacteria can modify their lipid A with positively charged moieties (e.g., 4-amino-4-deoxy-L-arabinose, phosphoethanolamine, and/or galactosamine) or hydrophobic groups (e.g., deacylation and palmitoylation) to reduce the interaction.[5,8,9] Notably, *A. baumannii* strains can also prevent themselves from being killed by polymyxins by losing LPS.[10,11] Intriguingly, some LPS-deficient *A. baumannii* isolates show a non-culturable phenotype on agar in the absence of polymyxins, displaying polymyxin-dependent resistance.[12–14] Polymyxin-dependent *A. baumannii* strains are highly clinically relevant, and recent clinical studies revealed that 32.9% of 149 colistin-susceptible *A. baumannii* clinical isolates developed polymyxin dependence.[12] Critically, unculturable polymyxin-dependent *A. baumannii* strains are not detected with the culture-based

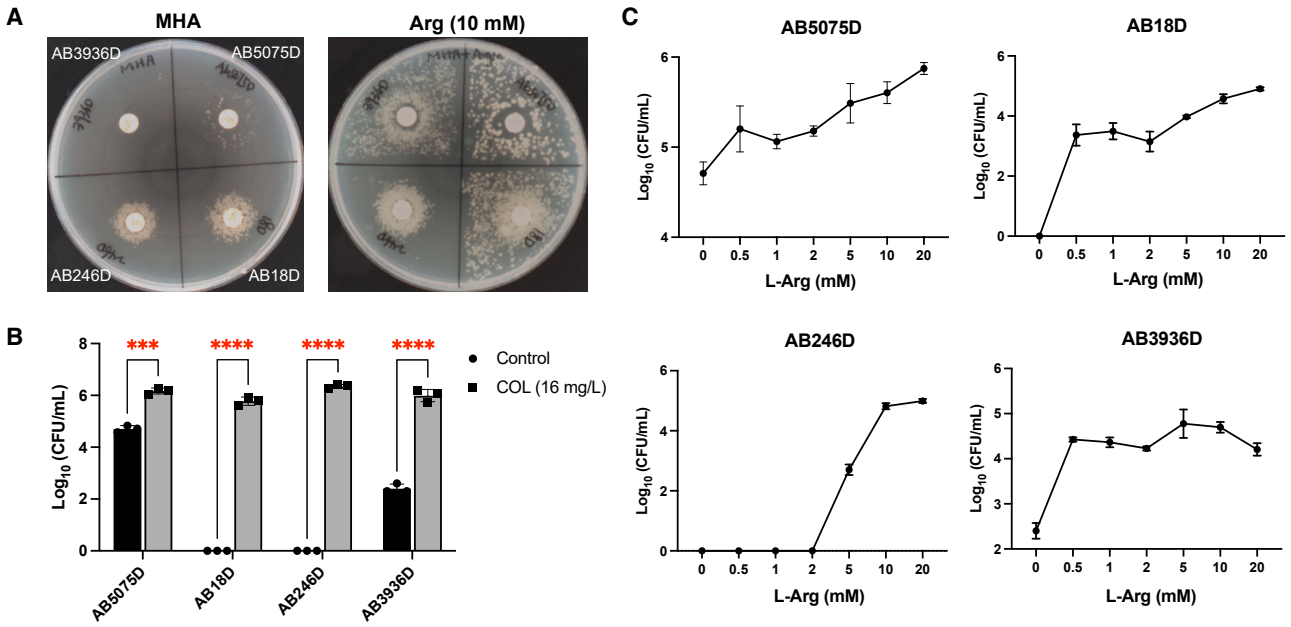

Figure 1. Arginine supplementation improved the diagnosis of polymyxin-dependent *A. baumannii* on MH agar

(A) Bacterial growth of polymyxin-dependent strains in the absence (left) or presence (right) of 10 mM L-arginine with 10 μg colistin on the paper disc.

(B) Bacterial colony counts in the absence or presence of 16 mg/L colistin. ***$p < 0.001$ and ****$p < 0.0001$ (unpaired t test).

(C) Bacterial colony counts in the presence of L-arginine at 0–20 mM.

All data in (B) and (C) were collected based on three independent biological replicates and are represented as mean ± SD.

diagnostic methods currently used in hospital clinical microbiology laboratories, resulting in a high rate of treatment failure in patients.[12,13]

Previous studies have shown that LPS deficiency in *A. baumannii* can be mediated by mutations in the *lpxA/C/D* genes, which encode the first enzymes of the lipid A biosynthesis pathway.[10,14] LPS loss leads to significant transcriptional perturbations associated with outer membrane remodeling, including increased transcription of genes encoding cell envelope biogenesis, lipoproteins, and the lipoprotein transport system.[15] Disruption of proteins involved in outer membrane asymmetry maintenance, specifically Mla (maintaining lipid asymmetry through retrograde phospholipid transport) and PldA (an outer membrane phospholipase), enhances growth fitness in LPS-deficient *A. baumannii*.[16] Our group recently discovered an increased proportion of phosphatidylglycerol (PG; a predominant phospholipid in bacterial membranes) in the outer membrane of LPS-deficient, polymyxin-dependent *A. baumannii*, which is essential to form "patch" binding by the polymyxin molecules through polar interaction between the cationic polymyxins and anionic PG head groups.[17] In this instance, instead of disrupting the outer membrane, polymyxin molecules strengthen membrane integrity and protect bacterial cells against external reactive oxygen species (ROS), producing a polymyxin-dependent phenotype. However, the key genes and metabolites contributing to the polymyxin dependence in *A. baumannii* strains remain unknown. Importantly, since polymyxin-dependent strains are "undetectable" on commonly used agar plates in the absence of polymyxins, they cannot be detected in the current culture-based diagnosis laboratories in hospitals. These major knowledge gaps have severely limited our understanding of polymyxin-dependent resistance and hindered the selection of effective therapeutic options for this unique type of pathogen.

In the present study, we integrated multi-omics to examine the mechanism of polymyxin-dependent growth in *A. baumannii* and identified significant perturbations in the arginine degradation pathway. Our study demonstrates that exogeneous arginine is required for polymyxin-dependent *A. baumannii* to fortify the integrity of its outer membrane. Our findings emphasize the significance of identifying polymyxin-dependent *A. baumannii* in clinical microbiology laboratories for the effective treatment of this challenging pathogen.

RESULTS

Phenotypic characterization of polymyxin-dependent *A. baumannii* isolates

Four LPS-deficient, polymyxin-dependent strains, AB18D, AB246D, AB3936D, and the recently reported AB5075D[17] were obtained from *A. baumannii* clinical isolates in our laboratory (Figures 1A and S1A). These polymyxin-dependent strains were all highly resistant to colistin, with minimum inhibitory concentrations (MICs) >256 mg/L, compared to their isogenic polymyxin-susceptible wild-type strains (MICs: 0.5 mg/L for AB5075, AB18S, and AB246S; 1.0 mg/L for AB3936S). The presence of 16 mg/L colistin enhanced the bacterial counts of the polymyxin-dependent strains by at least 1.5-$\log_{10}$ colony-forming units (CFU)/mL compared to those without colistin (Figures 1B and S1B). Notably, despite exhibiting attenuated virulence,[11,18]

Table 1. Polymyxin-dependent strains used in the present study

Wild-type strain	Colistin MIC (mg/L)	Polymyxin-dependent strain	Colistin MIC (mg/L)	Mutation
AB5075	0.5	AB5075D	>256	IS*Aba1* insertion at 395 nt of *lpxC*, ABUW_0135^{S25*}, *mrcA*^{M129T}, *katG*^{R609G}, and *rpoB*^{F915L}
AB18S	0.5	AB18D	>256	*mlaA*^{V184fs}, *pmrB*^{R263C}, and *lpxA*^{A141V}
AB246S	0.5	AB246D	>256	IS*Aba1* insertion at 375 nt of *lpxC*
AB3936S	1	AB3936D	>256	*lpxC*^{G35*}

The genome of AB5075D has been reported previously.[17]

all polymyxin-dependent strains (including AB5075D) caused infection in the thighs of neutropenic mice that persisted even after treatment with colistin (30 mg/kg/6 h for 18 h; Figure S2).[17] Therefore, it is critical to improve the diagnosis of undetectable polymyxin-dependent bacteria for optimizing treatment and facilitating the development of novel therapeutics.

We subsequently examined whether common exogenous nutrients could impact the growth of these polymyxin-dependent strains in the absence of polymyxins. Cultures of each strain were individually supplemented with different amino acids and carbon/nitrogen sources on Mueller-Hinton (MH) agar (Figure S3). Our findings revealed that only arginine supplementation substantially enhanced the growth of all four polymyxin-dependent strains but not their wild-type strains (Figures 1C, S3, and S4). These results indicated the potential of arginine to enhance the diagnosis of problematic undetectable polymyxin-dependent strains. Next, our study focused on the molecular mechanism of arginine-facilitated growth fitness in polymyxin-dependent *A. baumannii* strains.

Significant genes and metabolites associated with polymyxin dependence

Whole-genome sequencing identified 3 non-synonymous substitutions (*pmrB*^{R263C}, *lpxA*^{A141V}, and *mlaA*^{V184fs}) in AB18D, a transposon insertion at nucleotide position 375 of *lpxC* in AB246D, and a stop-gain mutation in *lpxC*^{Gly35*} in AB3936D (Tables 1 and S1). Mutations in the first two genes of lipid A biosynthesis, namely *lpxA* and *lpxC*, abolish lipid A biosynthesis and result in an LPS-deficient phenotype.[19] The absence of lipid A in all polymyxin-dependent strains in the present study was confirmed by lipid A profiling (Figure S5). Phylogenetic analysis of the whole-genome sequences and individual *lpxA* and *lpxC* genes from 15,049 *A. baumannii* strains in the GenBank database showed that AB5075 (named AB5075S in this paper), AB246S, and AB3936S were closely related but were not so with AB18S (Figures 2A and S6A).

To understand the key genes responsible for the polymyxin-dependent growth in *A. baumannii*, we conducted a transcriptomic analysis comparing all four polymyxin-dependent strains with their respective wild-type strains (Figure S6B). Our data revealed many differentially expressed genes (DEGs; 206/219 [increased/decreased] in AB5075D, 155/160 in AB18D, 219/461 in AB246D, and 182/269 in AB3936D; fold change [FC] > 2 and false discovery rate [FDR] < 0.05) (Figure S6C). Further analyses showed 38 common DEGs associated with several biochemical pathways in all four mutant/parent groups (Figure S6D). Notably, upregulated expressions of genes associated with arginine biosynthesis (ABUW_3850, 3851, and *argA*) and degradation (*astADB*) were uniquely identified across all polymyxin-dependent strains (Figure 2B). However, colistin treatment only induced minimum changes in the transcriptome of the four polymyxin-dependent strains (Figure S6C).

Comparative metabolomics was simultaneously conducted with the same samples that were subjected to the transcriptomics analysis described above. The findings revealed major metabolic differences between the polymyxin-dependent and wild-type strains, with the presence of 16 mg/L colistin transitioning the metabolome of the polymyxin-dependent strains closer to that of their parent strains (Figure S7A). Specifically, the numbers of altered metabolites (increased/decreased; FC > 2 and FDR < 0.05) for each polymyxin-dependent strain relative to its susceptible wild-type strain were 13/49 in AB5075D, 116/180 in AB18D, 48/168 in AB246D, and 45/165 in AB3936D (Figure S7B, top). This included 33 common metabolites that were significantly altered in all four pairs of bacterial strains examined (Figure S7C, top). Interestingly, treatment of polymyxin-dependent strains with 16 mg/L colistin for 2 h generally increased the levels of most metabolites and resulted in 60/11 altered metabolites (increased/decreased; FC > 2 and FDR < 0.05) in AB5075D, 131/13 in AB18D, 48/8 in AB246D, and 119/59 in AB3936D (Figure S7B, bottom), 18 of which were commonly changed in all four pairs of bacterial strains (Figure S7C, bottom). Notably, consistent with our transcriptomic results, a large proportion among these commonly changed metabolites was associated with arginine and glutamate metabolism (Figure 2C). Our pathway enrichment and network analysis with significantly changed genes and metabolites across all four polymyxin-dependent strains further highlighted the critical impact of arginine and glutamate metabolism on polymyxin dependence (Figures 2D, 2E, and S8). Specifically, metabolites associated with arginine biosynthesis (including L-glutamate, *N*-acetyl-glutamate, L-ornithine, and L-citrulline) and degradation (including L-arginine, N^2-succinyl-L-arginine, and L-glutamate) were significantly decreased in the polymyxin-dependent strains compared to their parent strain in the absence of colistin; conversely, they increased in the presence of 16 mg/L colistin (Figure 3).

Arginine supplementation enhanced metabolic activity in polymyxin-dependent *A. baumannii*

As the correlative transcriptomics and metabolomics results identified significantly perturbed arginine metabolism, we

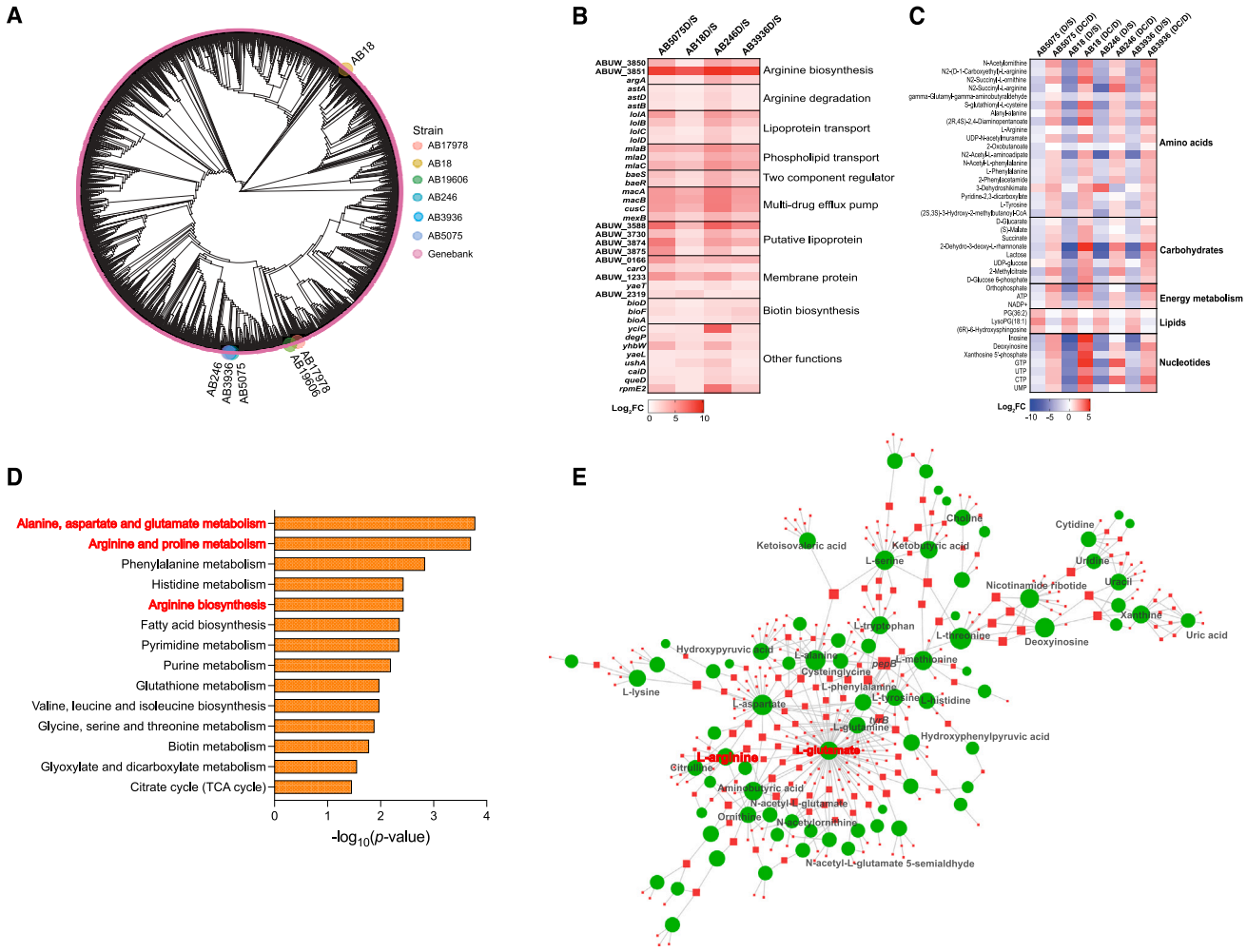

Figure 2. Genomic, transcriptomic, and metabolomic analyses of polymyxin-dependent *A. baumannii* strains

(A) Clustering analysis of the whole genome of 15,049 *A. baumannii* strains from GenBank and the wild-type strains of the four polymyxin-dependent strains in the present study.

(B) Heatmap showing the fold changes of common DEGs in all four polymyxin-dependent strains compared to their parent strains.

(C) Heatmap showing commonly changed metabolites in polymyxin-dependent strains compared to their wild-type strains following treatment with 16 mg/L colistin for 2 h in dependent strains plus untreated control. S, polymyxin-susceptible parent strains (no colistin treatment); D, polymyxin-dependent strains (no colistin treatment); DC, polymyxin-dependent strains treated with 16 mg/L colistin.

(D) Pathway enrichment analysis of the integrative transcriptomics and metabolomics data in all four polymyxin-dependent strains compared to their wild-type strains.

(E) Network analysis of the significant metabolites (green circle) and genes (red square) in all four polymyxin-dependent strains compared to their wild-type strains. Only metabolites/genes with a network degree >5 are labeled.

The pathway analysis in (D) and (E) was based on the KEGG Database and performed with MetaboAnalyst[20] and OmicsNet,[21] respectively.

hypothesized that exogenous supplementation of arginine improves the metabolic activity of the polymyxin-dependent strains and enhances their growth (Figures 1A and 1C). Therefore, we cultured polymyxin-dependent strains in M9 media with arginine as the sole carbon source to avoid the impact caused by complex nutrients in rich medium (Figure 4A). As AB5075S is a model strain and AB18S displayed the most phylogenetic difference among all four wild-type strains, their polymyxin-dependent strains AB5075D and AB18D were selected as the representative strains. Both polymyxin-dependent strains grew much faster than their wild-type strains, confirming that growth of these defective bacterial cells is dependent on the presence of arginine (Figure 4A). Importantly, in contrast to the upregulation of the *astA/B/D/E* genes in the polymyxin-dependent bacteria observed in a rich media cation-adjusted MH broth without arginine supplementation, their expression (especially in AB18D) in the minimal M9 media (with arginine as the sole carbon source) was downregulated compared to their parental strains (Figure 4B). Furthermore, our stable isotope labeling data with AB5075D as a representative strain confirmed that the uptake

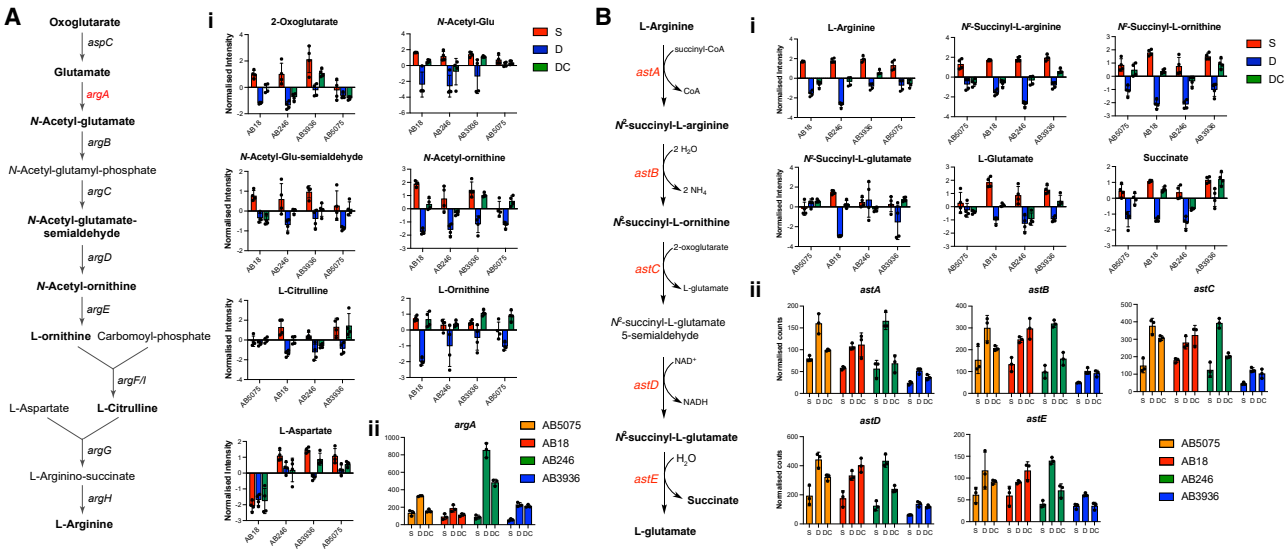

Figure 3. Significant perturbations of major metabolites and genes in arginine synthesis and degradation pathways

(A) Arginine synthesis pathway.

(B) Arginine degradation pathway.

(Ai and Bi) Metabolites.

(Aii and Bii) Genes.

A total of 4 biological replicates were conducted in the metabolomics study and 3 biological replicates in the transcriptomics study. All data are represented as mean ± SD. S, wild-type polymyxin-susceptible strains (no colistin treatment); D, polymyxin-dependent strains (no colistin treatment); DC, polymyxin-dependent strains treated with 16 mg/L colistin for 2 h.

of fully labeled $^{13}C_6$-L-arginine was very rapid, reaching a plateau (relative labeling > 90%) within approximately 15 min (Figures 4C and S9A). However, the intracellular abundance of $^{13}C_6$-L-arginine was much higher (FC > 2, $p < 0.05$) in AB5075D in the absence or presence of 16 mg/L colistin compared to its parent AB5075S at early time points 0.25–1 h, while it reached a similar level at 2 h (Figure 4C). Consistent with the uptake of $^{13}C_6$-L-arginine, the relative incorporation of ^{13}C into its downstream products in the arginine degradation pathway, namely N^2-succinyl-L-arginine (sum of labeled forms of 6–10 carbons) and N^2-succinyl-L-ornithine (sum of labeled forms of 5–9 carbons), also plateaued within 15 min (Figures S9A and S9B). Notably, the generation of fully labeled $^{13}C_5$-L-glutamate was significantly higher in AB5075D compared to AB5075S, with 61.2% ± 6.8% and 65.6% ± 5.0% of carbons fully labeled in AB5075D at 15 min in the absence or presence of 16 mg/L colistin, respectively, while only 37.9% ± 2.5% of carbons fully labeled in AB5075S in the absence of colistin ($p < 0.05$; AB5075D or AB5075DC vs. AB5075S). The higher incorporation of $^{13}C_5$-L-glutamate in AB5075D compared to AB5075S was maintained over the 2-h experimental period ($p < 0.05$; Figure 4C). Collectively, our results revealed that the polymyxin-dependent strain consumed a higher level of arginine and underwent faster arginine degradation than its wild-type strain, which clearly indicates that arginine increases the metabolic activity in polymyxin-dependent *A. baumannii*.

We have previously shown that polymyxin-dependent bacteria with defective outer membranes experienced much higher oxidative stress compared to wild-type strains.[17] In the present study, flow cytometry analysis (Figure S9C) revealed that supplementation with arginine decreased the production of ROS in the polymyxin-dependent strains at 30 (with the exception of AB3936D) and 90 (all four strains) min. This is very likely due to membrane protection by arginine supplementation in these strains, as their membrane potential was also rescued under the same condition (Figure S9D). Consistently, the antioxidative compounds spermine and spermidine (which are derived from arginine), and glutathione, also improved the growth of all the polymyxin-dependent strains (Figure S9E).

The *ast* operon is critical for polymyxin dependence in *A. baumannii*

To examine how arginine metabolism affects polymyxin dependence in AB5075D, we made a clean deletion of *astA*, which encodes an *N*-succinyltransferase, the first enzyme in the arginine degradation pathway (Table S2).[22] The *astA* deletion mutant of AB5075D, namely AB5075D$^{\Delta astA}$, was confirmed by PCR and whole-genome sequencing, showing no additional mutations compared to its parent AB5075D (Table S3; Figures S10A and S10B). Furthermore, inactivation of *astA* or other genes (e.g., *astB*/*D*/*E*) in the *ast* operon resulted in no bacterial growth in M9 media when arginine served as the sole carbon source (Figure S10C). As AB5075D and AB5075D$^{\Delta astA}$ contained insertional inactivation of *lpxC* by IS*Aba1* (Table S3; Figure S10D), neither AB5075D nor AB5075D$^{\Delta astA}$ produced any of the lipid A molecules present in the wild-type AB5075S (Figure S10E). Intriguingly, we observed that AB5075D$^{\Delta astA}$ grew significantly better than AB5075D and produced less ROS with rescued membrane potential (Figures 5A, 5B, and S10F). Compared to AB5075D, whose growth was significantly reduced by the presence of 8 mg/L H_2O_2 (2 × MICs against AB5075D), the growth of AB5075D$^{\Delta astA}$

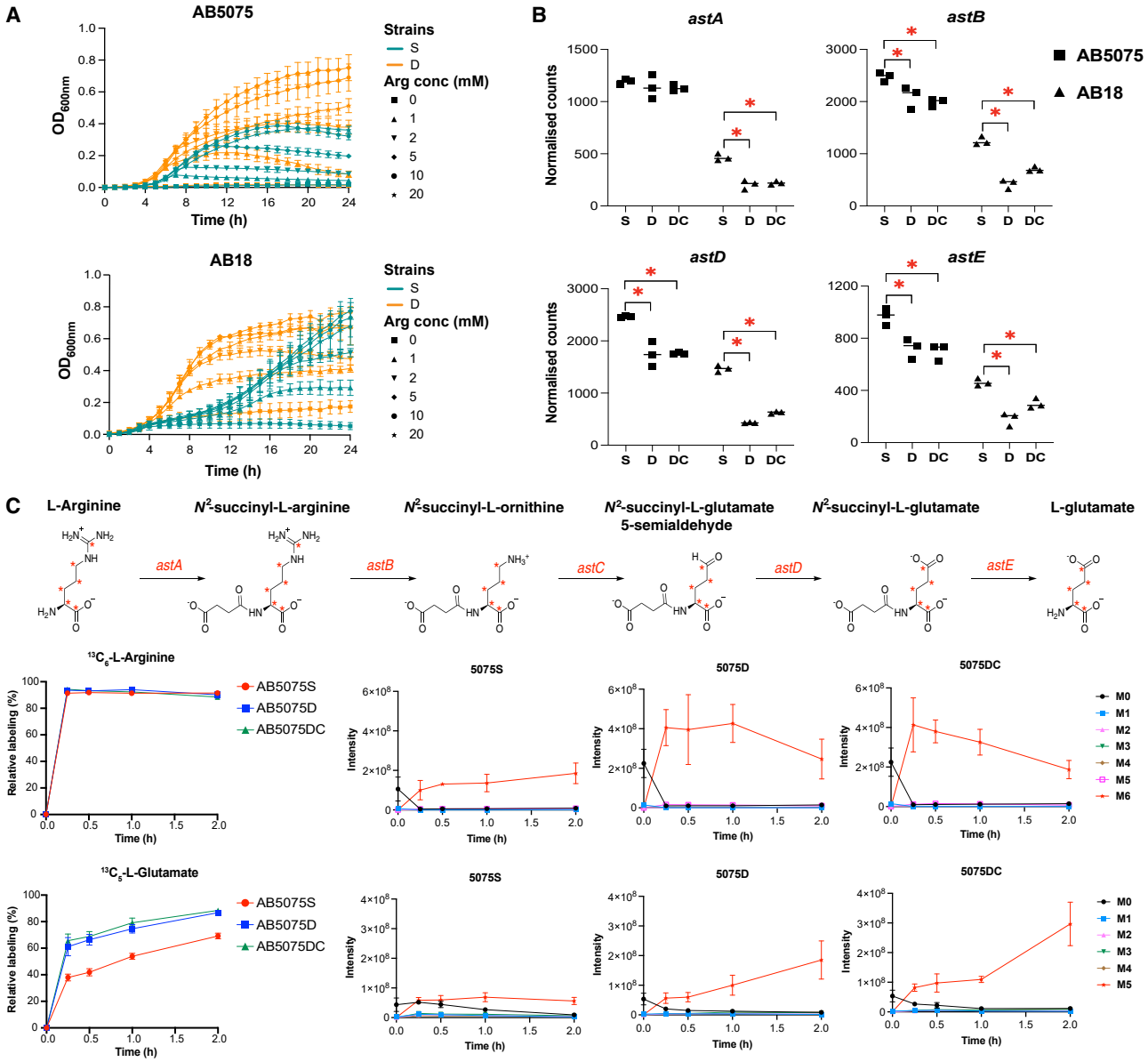

Figure 4. Arginine supplementation enhanced metabolic activity in polymyxin-dependent *A. baumannii*

(A) Bacterial growth of AB5075S/D and AB18S/D in M9 media with arginine (0–20 mM) as the sole carbon source.

(B) Expression of *astA/B/D/E* genes in the *ast* operon in polymyxin-dependent strains (AB5075D and AB18D) with or without 16 mg/L colistin for 2 h compared to their polymyxin-susceptible wild-type strains (AB5075S and AB18S). *$p < 0.05$ (two-way ANOVA with Tukey's correction).

(C) ^{13}C-labeling study of the arginine degradation pathway showing the relative labeling kinetics of the fully labeled $^{13}C_6$-L-arginine and $^{13}C_5$-L-glutamate and their intensity change across 2 h. S, polymyxin-susceptible wild-type strains (no colistin treatment); D, polymyxin-dependent strain (no colistin treatment); DC, polymyxin-dependent strains treated with 16 mg/L colistin. The labels M0, M1 … Mn indicate the number of carbons (0, 1 … n) labeled with ^{13}C. All data were collected from M9 culture with three independent biological replicates and are represented as mean ± SD.

was less affected by H_2O_2 (Figure 5C). Moreover, compared to AB5075D, AB5075D$^{\Delta astA}$ showed reduced polymyxin dependence on nutrient agar, albeit still retaining polymyxin resistance (colistin MICs > 256 mg/L) (Figures 5A and S10G). Our transcriptomics analysis showed that the expression of *astB/D/E* genes was significantly decreased ($log_2FC < -1$) in AB5075D$^{\Delta astA}$ compared to AB5075D (Figure S11A). Additionally, genes associated with glutamate metabolism (e.g., *aspA*; $log_2FC = -1.2$) and H_2O_2 degradation (e.g., *katG*; $log_2FC = -0.7$) were also significantly downregulated, while *argO* (involved in arginine excretion) was upregulated in AB5075D$^{\Delta astA}$, compared to AB5075D (Figure S11B). Significantly lower levels of N^2-succinyl-L-arginine, N^2-succinyl-L-ornithine, and L-ornithine were also consistently observed in AB5075D$^{\Delta astA}$ compared to AB5075D (Figure S11C).

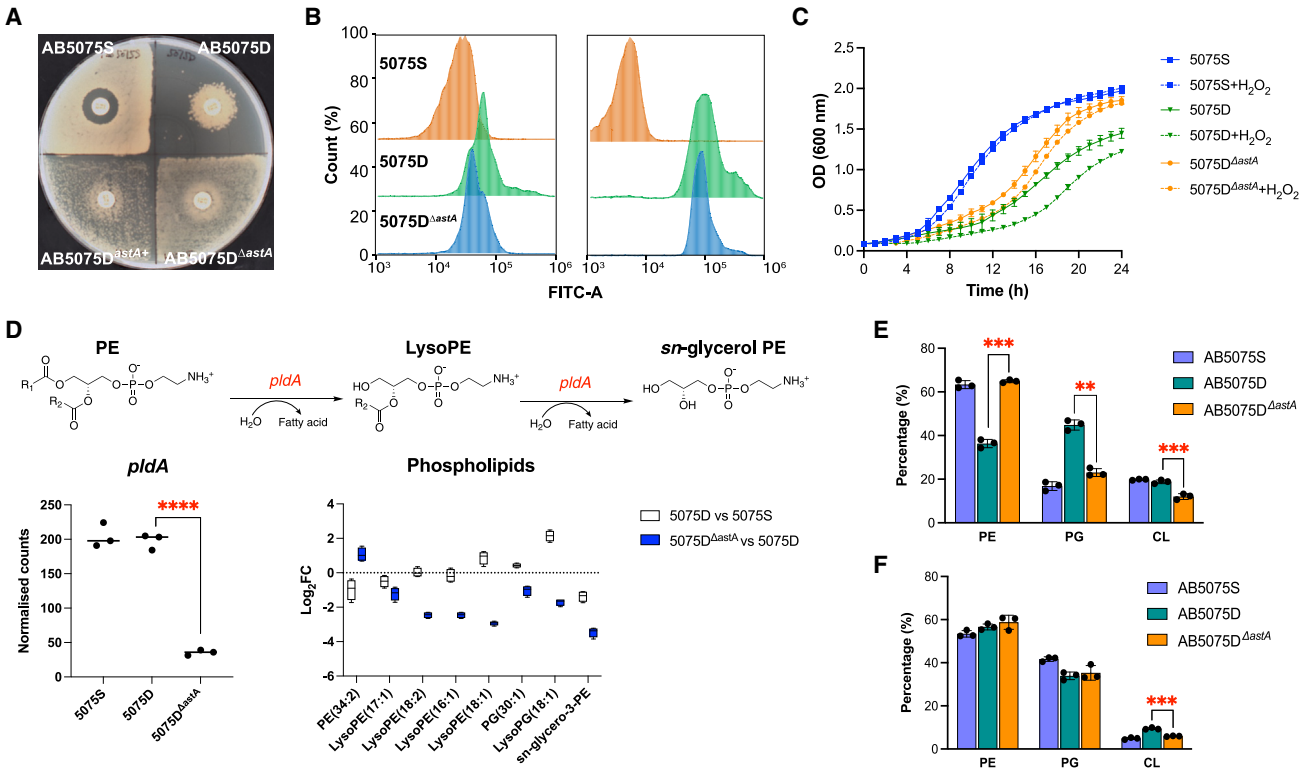

Figure 5. Significant effects of *astA* deletion in polymyxin-dependent AB5075D

(A) Growth of the *astA* deletion and complementation mutants (i.e., AB5075D$^{\Delta astA}$ and AB5075D^{astA+}, respectively) on MH agar with discs containing 10 μg colistin.

(B) Measurement of cellular ROS production (left) and membrane potential (right) of AB5075S (5075S), AB5075D (5075D), and AB5075D$^{\Delta astA}$ (5075D$^{\Delta astA}$).

(C) Growth of AB5075S (5075S), AB5075D (5075D), and AB5075D$^{\Delta astA}$ (5075D$^{\Delta astA}$) in the absence (solid curves) or presence (dashed curves) of 8 mg/L H_2O_2 in cation-adjusted MH broth (CAMHB) (n = 3).

(D) Transcriptomic and metabolic changes of phospholipid (PL) metabolism in AB5075D$^{\Delta astA}$ compared to AB5075D and the wild-type strain AB5075S. ****$p < 0.0001$ (one-way ANOVA with Tukey's correction) (only showed the significance in AB5075D$^{\Delta astA}$).

(E and F) Proportion of major PLs in the (E) outer membrane (OM) and (F) inner membrane of AB5075S, AB5075D, and AB5075D$^{\Delta astA}$. PE, phosphatidylethanolamine; PG, phosphatidylglycerol; CL, cardiolipin. **$p < 0.01$ and ***$p < 0.001$ (two-way ANOVA with Tukey's correction). All data displayed in the bar charts are represented as mean ± SD, with only the significance between AB5075D and AB5075D$^{\Delta astA}$ displayed.

astA deletion perturbed OM phospholipids and affected membrane interaction with polymyxins

As it has been suggested that improved phospholipid homeostasis in the outer membrane of LPS-deficient *A. baumannii* can result in growth benefits,[16] we hypothesized that the outer membrane of AB5075D underwent alterations due to *astA* deletion. Compared to AB5075D, our transcriptomics and metabolomics results with AB5075D$^{\Delta astA}$ revealed the significantly decreased expression of *pldA* ($\log_2$FC = −2.50, $p < 0.0001$) and the decreased abundance of lyso-phosphatidylethanolamine (lysoPE; $\log_2$FC < −1, $p < 0.05$) and *sn*-glycerol phosphoethanolamine ($\log_2$FC = −3.43, $p < 0.0001$) (Figure 5D). These data suggested an increased level of PE. Moreover, closely related to phospholipid metabolism, our data showed significantly reduced expression of genes related to fatty acid β-oxidation (e.g., ABUW_0374, *fadA* and *fadB*) and decreased levels of fatty acids (e.g., palmitic acid, palmitoleic acid, and phytanic acid) in AB5075D$^{\Delta astA}$ compared to AB5075D (Figure S12). These results indicate that the polymyxin-dependent bacteria enhance their phospholipid biogenesis via inhibiting fatty acid degradation and increasing the incorporation of fatty acyls. Our subsequent lipidomics analysis of the membrane fractions supported our hypothesis, revealing dramatic perturbations between the outer membrane lipids of AB5075D$^{\Delta astA}$ and AB5075D (Figure S13A). Specifically, the proportion of PG significantly decreased (from 44.8% to 23.0%) and that of PE significantly increased (from 36.3% to 64.9%) in the outer membrane of AB5075D$^{\Delta astA}$, relative to AB5075D ($p < 0.01$; Figures 5E, S13B, and S13C). These lipidomic changes transitioned the outer membrane lipid proportions in AB5075D$^{\Delta astA}$ to a level similar to that in the wild-type AB5075S (16.8% PG and 63.4% PE). In contrast, the proportions of PG and PE in the inner membrane did not significantly change in AB5075D$^{\Delta astA}$ compared to AB5075D (Figure 5F).

To confirm the impact of *astA*-mediated phospholipid proportion change on the interaction with polymyxins, we firstly performed all-atom molecular dynamics (MD) simulations using our lipidomics data above (Figures 6A and 6B; Table S4; Videos S1 and S2). The tail region of colistin molecules

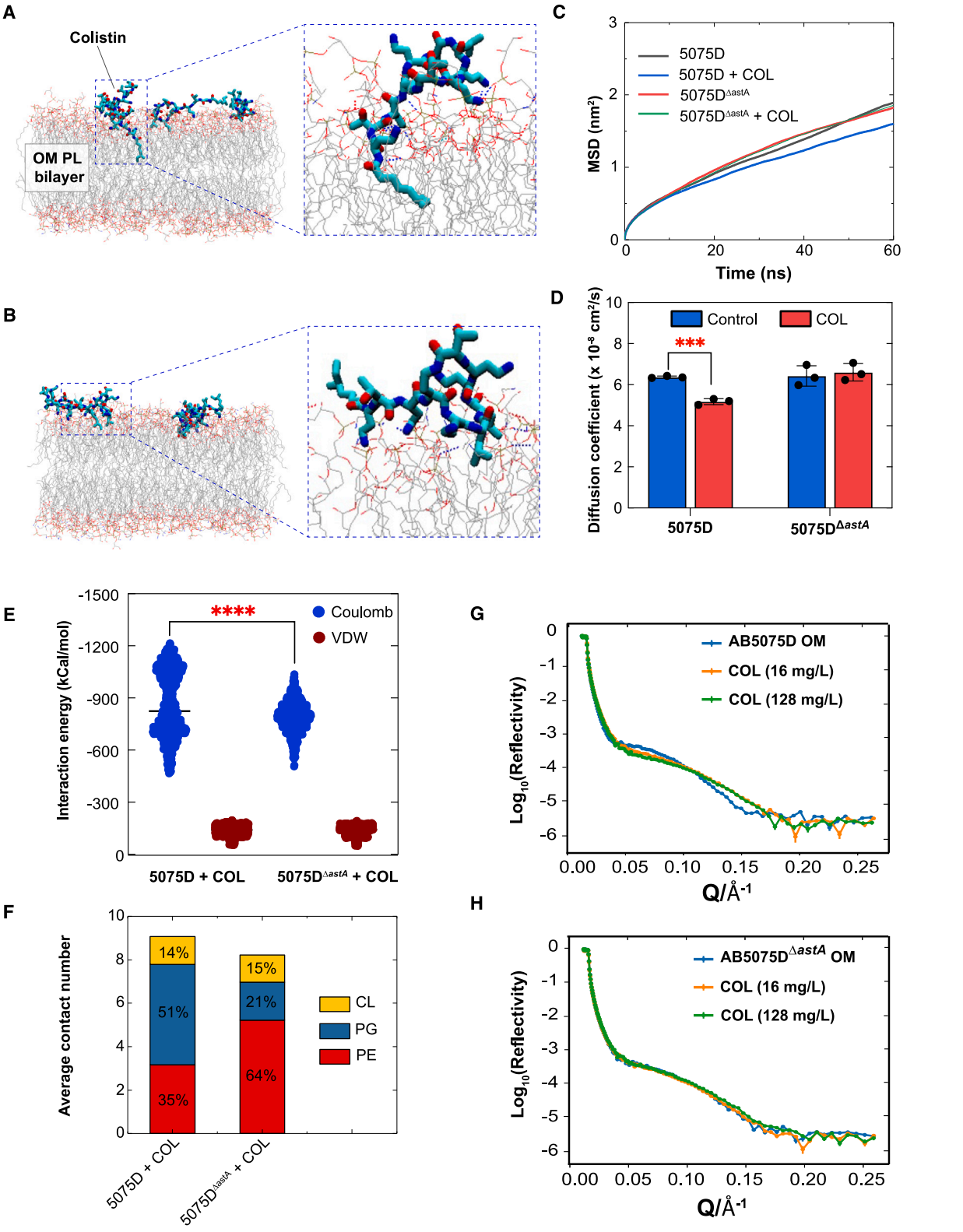

(legend on next page)

inserted into the model outer membrane of the polymyxin-dependent strain AB5075D (Video S1) but not its *astA* deletion mutant AB5075D$^{\Delta astA}$ (Video S2). Colistin decreased the movement of the binding phospholipids, resulting in a significantly reduced lateral diffusion coefficient (from 6.43 × 10^{-8} to 5.20 × 10^{-8} cm^2s^{-1}) in the outer membrane of AB5075D (Figures 6C and 6D). In contrast, only minimum changes in this coefficient were observed in AB5075D$^{\Delta astA}$ (from 6.34 × 10^{-8} to 6.52 × 10^{-8} cm^2s^{-1}) (Figures 6C and 6D). As colistin molecules interact more with the negatively charged PG than PE and cardiolipin,[17] our MD data confirmed that the decreased proportion of PG (from 44.8% to 23.0%) in the outer membrane of AB5075D$^{\Delta astA}$ led to a weaker interaction with colistin compared to AB5075D. This is evidenced by the increased electrostatic interaction energy (−791.7 vs. −862.5 kJ/mol) and decreased interacting phospholipids per colistin molecule (8.2 vs. 9.1) (Figures 6E and 6F).

To further investigate the impact of phospholipid change on polymyxin interaction, we next conducted a neutron reflectometry (NR) study (Figure S14A). NR provides nanoscale-resolution spatial information on biological membranes and resolves the location and orientation of antimicrobial peptides in membranes in a non-destructive manner.[23–25] Our NR results showed a relative volume fraction of approximately 36% of colistin bound to the outer membrane surface of AB5075D, causing substantial changes to neutron reflectivity (Figures 6G, S14B, top and middle, and S14C; Tables S5 and S6). However, colistin did not cause any significant change to the outer membrane of the *astA* deletion mutant AB5075D$^{\Delta astA}$ (Figures 6H, S14B, bottom, and S14C; Table S7).

Collectively, our study showed that the deletion of *astA* in the polymyxin-dependent strain caused a significant change in the composition of phospholipids in the outer membrane, thereby decreasing the interaction with colistin. Our findings highlight that intracellular arginine metabolism and outer membrane lipid remodeling play a major role in the polymyxin-dependent growth of *A. baumannii*.

DISCUSSION

Polymyxin-dependent resistance serves as a perfect example of the Eagle effect[26] and has been overlooked in the clinic due to the non-culturable nature of these strains on agar in the absence of polymyxins. Worryingly, polymyxin-dependent *A. baumannii* is able to cause bloodstream infections, and treatment may fail even with the use of last-line polymyxins.[12] Therefore, improving the diagnosis of polymyxin-dependent strains is urgently required to optimize antibiotic treatment of infections caused by these undetectable isolates. Here, we demonstrated that arginine significantly improves growth of polymyxin-dependent *A. baumannii* and reduces polymyxin dependence (Figure 1). To understand the mechanism of polymyxin dependence and how arginine improves the diagnosis of polymyxin-dependent strains, we firstly employed an integrative systems pharmacology approach to investigate four polymyxin-dependent *A. baumannii* strains. Notably, our phylogenetic analysis showed that these strains were from various genetic linages (Figure 2A), and our whole-genome sequencing data confirmed that LPS loss is essential for the acquisition of polymyxin dependence (Table S1). The significant upregulation of genes involved in the transport of phospholipids (e.g., *mlaBCD*) and lipoproteins (e.g., *lolABCD*), two-component systems (e.g., *baeSR*), multidrug efflux pumps (e.g., *macAB*), and biotin synthesis (e.g., *bioADF*) across all four polymyxin-dependent strains strongly supports dramatic outer membrane remodeling due to LPS loss (Figure 2B).[9,10,15]

The most significant finding of our study is the upregulation of the *astABCDE* operon associated with arginine degradation in all four polymyxin-dependent *A. baumannii* strains (Figure 3B). This operon encodes enzymes in the arginine succinyltransferase (AST) pathway that converts arginine to glutamate, the major pathway for the utilization of arginine as a source of carbon, nitrogen, and energy.[27] By using transposon insertion and gene knockout mutants of AB5075, we demonstrated that the AST pathway is the only arginine degradation pathway in *A. baumannii* (Figure S10C). Furthermore, our metabolomics results showed that metabolites primarily involved in arginine biosynthesis and degradation were markedly depleted across all polymyxin-dependent strains relative to their parent strains (Figures 2C and 3). Interestingly, the levels of most of these metabolites were restored in the presence of colistin (16 mg/L) (Figure 3). Our screening of nutrient supplementation also highlighted the importance of arginine in enhancing bacterial growth and reducing polymyxin dependence (Figures 1A, 1C, and S3).

Also of note is that another amino acid, lysine, may also help improve the diagnosis of polymyxin-dependent bacteria (Figure S3). It is well known that lysine utilization within bacterial cells is closely associated with arginine metabolism, as both lysine and arginine can bind to the same proteins, including ArgT (for exporting arginine or lysine into cells), ArgO (for excreting arginine or lysine outside cells), and ArgP (for activating ArgO).[28] This further highlights the significance of arginine metabolism in enhancing bacterial diagnostics. When arginine served as the sole carbon source, the polymyxin-dependent strains

Figure 6. Molecular dynamics simulations and neutron reflectometry show different binding of polymyxins to the outer membrane of AB5075D and AB5075D$^{\Delta astA}$

(A and B) Molecular interactions between colistin (COL) and PL molecules in the outer membrane (OM) outer leaflet of (A) AB5075D and (B) AB5075D$^{\Delta astA}$.

(C) Mean square displacement (MSD) of each membrane system during the 60 ns simulation.

(D) Lateral diffusion coefficient of each OM with or without colistin. The coefficient value was calculated based on the slope of MSD. ***$p < 0.001$ (unpaired t test).

(E) Interaction energy between binding colistin and each membrane. Blue bars represent Coulomb interaction or electrostatic interaction, while red bars represent van der Waals interaction. ****$p < 0.0001$ (unpaired t test).

(F) Average number of interacting PE, PG, or CL per colistin molecule on the OM systems of AB5075D and AB5075D$^{\Delta astA}$.

(G and H) Neutron reflectometry profiles of the OM bilayers of (G) AB5075D and (H) AB5075D$^{\Delta astA}$ treated with 16 or 128 mg/L colistin compared to the untreated control in the D_2O contrast.

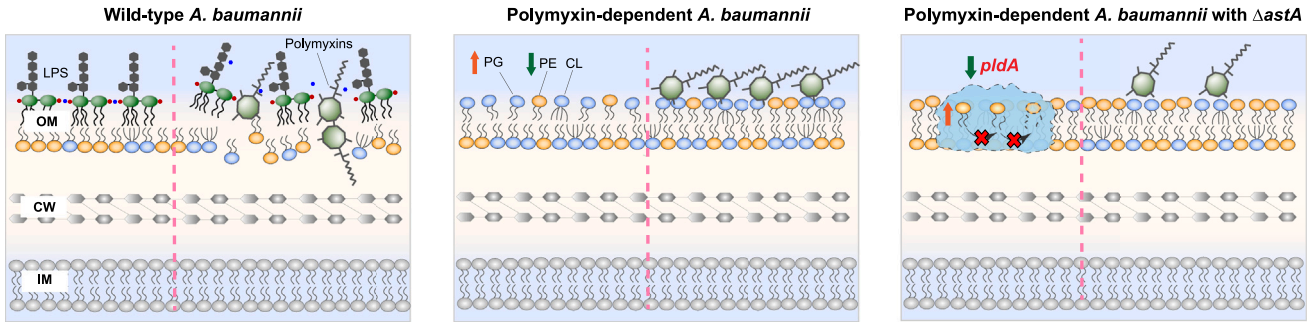

Figure 7. Model of the critical role of *astA* in polymyxin-dependent *A. baumannii*

(Left) Wild-type *A. baumannii* contains asymmetric OM architecture consisting of lipopolysaccharide (LPS) in the outer leaflet and phospholipids in the inner leaflet. When exposed to polymyxins (e.g., colistin), an electrostatic interaction was established between positively charged polymyxins and negatively charged LPS, resulting in OM disruption and cell death. (Center) In polymyxin-dependent *A. baumannii*, the OM was significantly remodeled due to LPS loss, with the proportion of phosphatidylglycerol (PG) increased. This led to increased net negative charge and intramolecular charge repulsion, resulting in an unstable OM. The presence of polymyxins caused patch binding with the PG-rich OM and increased OM integrity, resulting in a polymyxin-dependent phenomenon. (Right) *astA* deletion resulted in depletion of the OM phospholipase PldA, which prevented phospholipid degradation and led to an increased proportion of phosphatidylethanolamine (PE) in the OM of polymyxin-dependent bacteria. This adjustment brought the composition of OM phospholipids closer to that in the natural polymyxin-susceptible wild-type strains, thus reducing the excessive net negative charge. Consequently, the intramolecular charge repulsion within the OM was reduced, leading to a more stable OM architecture and weakened interaction with polymyxins. The pink dashed lines indicate the membrane status in the absence (left of the line) and presence (right) of polymyxins. OM, outer membrane; CW, cell wall; IM, inner membrane; CL, cardiolipin.

displayed significantly faster growth than their isogenic polymyxin-susceptible wild-type strains in M9 media (Figure 4A). Under this condition, the decreased expression of *ast* genes (e.g., in polymyxin-dependent AB18D; Figure 4B) reflected the increased arginine turnover in polymyxin-dependent strains. Moreover, our stable isotope labeling results demonstrated significantly higher uptake of L-arginine and faster generation of L-glutamate in polymyxin-dependent AB5075D compared to AB5075S (Figure 4C; $p < 0.05$). Collectively, we have shown that arginine supplementation increases metabolic activity and attenuates ROS production and membrane depolarization in polymyxin-dependent *A. baumannii* (Figures S9C and S9D). Therefore, arginine protects polymyxin-dependent strains by stabilizing their outer membrane and decreasing cellular oxidative stress. Indeed, arginine has been reported to reduce cellular ROS production in various bacterial species.[29,30]

Subsequently, we validated the critical role of arginine metabolism in polymyxin-dependent growth through a clean deletion of *astA* (the first gene in the arginine degradation pathway) in AB5075D. Construction of a clean deletion mutant in AB5075D was very challenging due to its high resistance to almost all common antibiotic selection markers and the lack of an optimized mutagenesis protocol for this model strain.[15,17] However, with the very limited choices of tetracycline and apramycin, a clean deletion of *astA* in AB5075D was achieved via a homologous recombination technique. Deletion of *astA* produced similar effects to arginine supplementation of AB5075D, namely substantial growth enhancement and decreased polymyxin dependence (Figure 5A). In accordance with *astA* deletion, expression of the downstream genes *astB/D/E* was severely decreased, thereby reducing the levels of related intermediates (e.g., N^2-succinyl-L-arginine and N^2-succinyl-L-ornithine) in the AST pathway (Figure S12), as observed in our metabolomics results.

Membrane lipidomics showed that compared to AB5075D, the proportion of PG was decreased while the proportion of PE increased in the outer membrane of AB5075D$^{\Delta astA}$, with the phospholipid level almost comparable to that in the wild-type AB5075S (Figure 5E). The downregulation of *pldA* (encoding a phospholipase located in the outer membrane) and decreased levels of lysoPE and *sn*-glycerol-PE indicated decreased PE degradation in AB5075D$^{\Delta astA}$ (Figure 5D). This agrees with the increased abundance of PE in the outer membrane of AB5075D$^{\Delta astA}$ (Figure 5E). Notably, we also observed significant downregulation of genes involved in fatty acid β-oxidation due to *astA* deletion (Figure S12), suggesting a potential link between arginine metabolism and the perturbation of membrane phospholipids. Our recent study revealed that polymyxin-dependent bacteria possess a significantly remodeled outer membrane with significantly higher PG abundance.[17] The increased proportion of PG explains the less stable outer membrane of polymyxin-dependent strains, as the negatively charged PG head groups result in significant intramolecular electrostatic repulsion. The latter is also demonstrated by the higher lateral diffusion of the outer membrane in the polymyxin-dependent strains compared to the wild-type polymyxin-susceptible strains.[17] This negatively charged environment in the outer membrane of polymyxin-dependent bacteria was critical for patch binding with the positively charged polymyxin molecules, which increases membrane integrity and leads to a polymyxin-dependent phenotype (Figure 7, middle).[17] It is well known that the outer membrane of gram-negative bacteria is usually rich in the zwitterionic PE (rather than PG) because of its unique cellular activities, including modulating membrane curvature,[31] acting as a lipochaperone,[32] and supporting membrane protein topogenesis (Figure 7, left).[33] Hence, the decreased PG (23.0%) and increased PE (64.9%) proportions in the outer membrane of the *astA* deletion mutant AB5075D$^{\Delta astA}$ restored phospholipids to a level similar to that in the outer membrane of the polymyxin-susceptible wild-type strains. This change led to a more stable outer membrane architecture and weakened its interaction with polymyxins,

diminishing the phenomenon of polymyxin dependence (Figure 7, right). This is in excellent agreement with our previous MD simulations study, which demonstrated that polymyxin molecules could only form patch binding with the outer membrane of *A. baumannii* and exhibit polymyxin dependence when the proportion of PG reached approximately 35% or higher.[17] Our current MD study further confirmed our hypothesis that the decreased proportion of PG (23.0%) in the outer membrane of AB5075D$^{\Delta astA}$ forms a weaker interaction with colistin compared to its parent AB5075D (Figures 6A–6F). Notably, NR results confirmed this finding, showing that the outer membrane of AB5075D$^{\Delta astA}$ displayed no significant interaction with colistin. This was evidenced by the absence of any obvious change in the reflectivity profile, in contrast to what was observed with AB5075D (Figures 6G, 6H, and S14C). To the best of our knowledge, this is the first study to report that the arginine degradation pathway plays a key role in outer membrane lipid remodeling in polymyxin-dependent *A. baumannii*, with the mechanism being investigated in our laboratory.

In conclusion, polymyxin-dependent strains are highly resistant to the last-line polymyxins and remain undetectable in clinical microbiology diagnostic laboratories. Here, we identified a novel mechanism whereby the "defective" polymyxin-dependent bacteria alter their arginine metabolic pathways, resulting in changes in their outer membrane composition compared to their isogenic wild-type parents. Understanding the mechanism underlying this unique polymyxin-dependent resistance is crucial for the detection of "invisible" polymyxin-dependent *A. baumannii* and optimizing antibiotic treatment of this life-threatening problematic pathogen.

Limitations of the study

This study demonstrated that arginine metabolism impacts membrane lipid composition in polymyxin-dependent *A. baumannii*. Transcriptomics revealed that genes involved in fatty acid β-oxidation (e.g., *fadA* and *fadB*) and the production of ROS (e.g., *katG*) were significantly downregulated in the *astA* deletion mutant AB5075D$^{\Delta astA}$ compared to its parent, AB5075D. A limitation of this study is that it remains to be determined how arginine metabolism affects fatty acid β-oxidation and ROS production and how these changes influence the composition of bacterial membrane lipids. Further investigations using molecular biology and metabolic fluxomics of arginine catabolism are being conducted in our laboratory to address both questions.

STAR★METHODS

Detailed methods are provided in the online version of this paper and include the following:

- KEY RESOURCES TABLE
- RESOURCE AVAILABILITY
  - Lead contact
  - Materials availability
  - Data and code availability
- EXPERIMENTAL MODEL AND STUDY PARTICIPANT DETAILS
  - Bacterial strains and culture
- METHOD DETAILS
  - Metabolite supplementation
  - Neutropenic murine thigh infection model
  - Whole genome sequencing
  - Comparative transcriptomics and metabolomics
  - Stable isotope labeling
  - Flow cytometry analysis
  - Construction of *astA* deletion and complementation in AB5075D
  - Membrane lipidomics and lipid A profiling
  - Molecular dynamic simulations
  - Neutron reflectometry measurement and data analysis
- QUANTIFICATION AND STATISTICAL ANALYSIS

SUPPLEMENTAL INFORMATION

Supplemental information can be found online at https://doi.org/10.1016/j.celrep.2024.114410.

ACKNOWLEDGMENTS

This research was supported by a research grant from the National Institute of Allergy and Infectious Disease (NIAID) of the National Institutes of Health (R01 AI132154). The content is solely the responsibility of the authors and does not necessarily represent the official views of NIAID. The NR experiment was supported by the Australian Nuclear Science and Technology Organisation through proposal P13566. The Spatz neutron beam instrument operations are funded through the National Collaborative Research Infrastructure Strategy (NCRIS), an Australian government initiative. M.-L.H. is an Australian Research Council (ARC) DECRA Fellow (DE230100356). D.J.C. is an ARC Future Fellow. N.A.P. is an Australian National Health and Medical Research Council (NHMRC) Early Career Research Fellow. J. Li is an Australian NHMRC Principal Research Fellow. The authors would like to thank the Monash Proteomics and Metabolomics Facility (Monash University), the Monash Micromon Genomics Facility (Monash University), and the Australian Nuclear Science and Technology Organisation (ANSTO) for providing technical support. We appreciate Prof. Denis Spelman (Alfred Hospital, Melbourne, Australia) and Dr. Jan Bell and Prof. John Turnidge (Women's and Children's Hospital, Adelaide, Australia) for providing the bacterial strains.

AUTHOR CONTRIBUTIONS

Conceptualization, M.-L.H. and J. Li; methodology, M.-L.H., Y.A., J.Z., X.J., R.A.D., C.K.B., D.J.C., and A.P.L.B.; investigation, M.-L.H., Y.A., J.Z., J. Lu, W.M., H.W., X.H., and Y.W.; resources, N.A.P., H.H.Y., and J.W.; formal analysis, M.-L.H., J.Z., and Y.Z.; writing – original draft, M.-L.H.; writing – review & editing, P.J.B., H.-H.S., T.L., D.J.C., T.V., and J. Li; supervision, J. Li; funding acquisition, J. Li.

DECLARATION OF INTERESTS

The authors declare no competing interests.

Received: November 3, 2023
Revised: February 3, 2024
Accepted: June 12, 2024
Published: June 25, 2024

REFERENCES

1. Dijkshoorn, L., Nemec, A., and Seifert, H. (2007). An increasing threat in hospitals: multidrug-resistant *Acinetobacter baumannii*. Nat. Rev. Microbiol. *5*, 939–951. https://doi.org/10.1038/nrmicro1789.
2. Harding, C.M., Hennon, S.W., and Feldman, M.F. (2018). Uncovering the mechanisms of *Acinetobacter baumannii* virulence. Nat. Rev. Microbiol. *16*, 91–102. https://doi.org/10.1038/nrmicro.2017.148.
3. (2024). WHO Bacterial Priority Pathogens List, 2024: bacterial pathogens of public health importance to guide research, development and strategies to prevent and control antimicrobial resistance (World Health Organization).

4. Karageorgopoulos, D.E., and Falagas, M.E. (2008). Current control and treatment of multidrug-resistant *Acinetobacter baumannii* infections. Lancet Infect. Dis. *8*, 751–762. https://doi.org/10.1016/S1473-3099(08)70279-2.

5. Nang, S.C., Azad, M.A.K., Velkov, T., Zhou, Q.T., and Li, J. (2021). Rescuing the last-line polymyxins: achievements and challenges. Pharmacol. Rev. *73*, 679–728. https://doi.org/10.1124/pharmrev.120.000020.

6. Nation, R.L., Velkov, T., and Li, J. (2014). Colistin and polymyxin B: peas in a pod, or chalk and cheese? Clin. Infect. Dis. *59*, 88–94. https://doi.org/10.1093/cid/ciu213.

7. Velkov, T., Thompson, P.E., Nation, R.L., and Li, J. (2010). Structure–activity relationships of polymyxin antibiotics. J. Med. Chem. *53*, 1898–1916. https://doi.org/10.1021/jm900999h.

8. Olaitan, A.O., Morand, S., and Rolain, J.-M. (2014). Mechanisms of polymyxin resistance: acquired and intrinsic resistance in bacteria. Front. Microbiol. *5*, 643. https://doi.org/10.3389/fmicb.2014.00643.

9. Simpson, B.W., and Trent, M.S. (2019). Pushing the envelope: LPS modifications and their consequences. Nat. Rev. Microbiol. *17*, 403–416. https://doi.org/10.1038/s41579-019-0201-x.

10. Henry, R., Vithanage, N., Harrison, P., Seemann, T., Coutts, S., Moffatt, J.H., Nation, R.L., Li, J., Harper, M., Adler, B., and Boyce, J.D. (2012). Colistin-resistant, lipopolysaccharide-deficient *Acinetobacter baumannii* responds to lipopolysaccharide loss through increased expression of genes involved in the synthesis and transport of lipoproteins, phospholipids, and poly-β-1,6-*N*-acetylglucosamine. Antimicrob. Agents Chemother. *56*, 59–69. https://doi.org/10.1128/AAC.05191-11.

11. Moffatt, J.H., Harper, M., Mansell, A., Crane, B., Fitzsimons, T.C., Nation, R.L., Li, J., Adler, B., and Boyce, J.D. (2013). Lipopolysaccharide-deficient *Acinetobacter baumannii* shows altered signaling through host Toll-like receptors and increased susceptibility to the host antimicrobial peptide LL-37. Infect. Immun. *81*, 684–689. https://doi.org/10.1128/IAI.01362-12.

12. Hong, Y.-K., Lee, J.-Y., Wi, Y.M., and Ko, K.S. (2016). High rate of colistin dependence in *Acinetobacter baumannii*. J. Antimicrob. Chemother. *71*, 2346–2348. https://doi.org/10.1093/jac/dkw121.

13. Hawley, J.S., Murray, C.K., and Jorgensen, J.H. (2007). Development of colistin-dependent *Acinetobacter baumannii*-*Acinetobacter calcoaceticus* complex. Antimicrob. Agents Chemother. *51*, 4529–4530. https://doi.org/10.1128/AAC.01115-07.

14. Lee, J.-Y., Chung, E.S., and Ko, K.S. (2017). Transition of colistin dependence into colistin resistance in *Acinetobacter baumannii*. Sci. Rep. *7*, 14216. https://doi.org/10.1038/s41598-017-14609-0.

15. Boll, J.M., Crofts, A.A., Peters, K., Cattoir, V., Vollmer, W., Davies, B.W., and Trent, M.S. (2016). A penicillin-binding protein inhibits selection of colistin-resistant, lipooligosaccharide-deficient *Acinetobacter baumannii*. Proc. Natl. Acad. Sci. USA *113*, E6228–E6237. https://doi.org/10.1073/pnas.1611594113.

16. Powers, M.J., and Trent, M.S. (2018). Phospholipid retention in the absence of asymmetry strengthens the outer membrane permeability barrier to last-resort antibiotics. Proc. Natl. Acad. Sci. USA *115*, E8518–E8527. https://doi.org/10.1073/pnas.1806714115.

17. Zhu, Y., Lu, J., Han, M.L., Jiang, X., Azad, M.A.K., Patil, N.A., Lin, Y.W., Zhao, J., Hu, Y., Yu, H.H., et al. (2020). Polymyxins bind to the cell surface of unculturable *Acinetobacter baumannii* and cause unique dependent resistance. Adv. Sci. *7*, 2000704. https://doi.org/10.1002/advs.202000704.

18. Kamoshida, G., Akaji, T., Takemoto, N., Suzuki, Y., Sato, Y., Kai, D., Hibino, T., Yamaguchi, D., Kikuchi-Ueda, T., Nishida, S., et al. (2020). Lipopolysaccharide-deficient *Acinetobacter baumannii* due to colistin resistance is killed by neutrophil-produced lysozyme. Front. Microbiol. *11*, 573. https://doi.org/10.3389/fmicb.2020.00573.

19. Zhang, G., Baidin, V., Pahil, K.S., Moison, E., Tomasek, D., Ramadoss, N.S., Chatterjee, A.K., McNamara, C.W., Young, T.S., Schultz, P.G., et al. (2018). Cell-based screen for discovering lipopolysaccharide biogenesis inhibitors. Proc. Natl. Acad. Sci. USA *115*, 6834–6839. https://doi.org/10.1073/pnas.1804670115.

20. Chong, J., Soufan, O., Li, C., Caraus, I., Li, S., Bourque, G., Wishart, D.S., and Xia, J. (2018). MetaboAnalyst 4.0: towards more transparent and integrative metabolomics analysis. Nucleic Acids Res. *46*, W486–W494. https://doi.org/10.1093/nar/gky310.

21. Zhou, G., and Xia, J. (2018). OmicsNet: a web-based tool for creation and visual analysis of biological networks in 3D space. Nucleic Acids Res. *46*, W514–W522. https://doi.org/10.1093/nar/gky510.

22. Kiupakis, A.K., and Reitzer, L. (2002). ArgR-independent induction and ArgR-dependent superinduction of the *astCADBE* operon in *Escherichia coli*. J. Bacteriol. *184*, 2940–2950. https://doi.org/10.1128/JB.184.11.2940-2950.2002.

23. Lakey, J.H. (2019). Recent advances in neutron reflectivity studies of biological membranes. Curr Opin Colloid In *42*, 33–40. https://doi.org/10.1016/j.cocis.2019.02.012.

24. Han, M.-L., Shen, H.-H., Hansford, K.A., Schneider, E.K., Sivanesan, S., Roberts, K.D., Thompson, P.E., Le Brun, A.P., Zhu, Y., Sani, M.-A., et al. (2017). Investigating the interaction of octapeptin A3 with model bacterial membranes. ACS Infect. Dis. *3*, 606–619. https://doi.org/10.1021/acsinfecdis.7b00065.

25. Lai, X., Ding, Y., Wu, C.-M., Chen, X., Jiang, J.-H., Hsu, H.-Y., Wang, Y., Le Brun, A.P., Song, J., Han, M.-L., et al. (2020). Phytantriol-based cubosome formulation as an antimicrobial against lipopolysaccharide-deficient gram-negative bacteria. ACS Appl. Mater. Interfaces *12*, 44485–44498. https://doi.org/10.1021/acsami.0c13309.

26. Prasetyoputri, A., Jarrad, A.M., Cooper, M.A., and Blaskovich, M.A.T. (2019). The Eagle effect and antibiotic-induced persistence: two sides of the same coin? Trends Microbiol. *27*, 339–354. https://doi.org/10.1016/j.tim.2018.10.007.

27. Schneider, B.L., Kiupakis, A.K., and Reitzer, L.J. (1998). Arginine catabolism and the arginine succinyltransferase pathway in *Escherichia coli*. J. Bacteriol. *180*, 4278–4286. https://doi.org/10.1128/jb.180.16.4278-4286.1998.

28. Charlier, D., and Bervoets, I. (2019). Regulation of arginine biosynthesis, catabolism and transport in *Escherichia coli*. Amino Acids *51*, 1103–1127. https://doi.org/10.1007/s00726-019-02757-8.

29. Tiwari, S., Van Tonder, A.J., Vilchèze, C., Mendes, V., Thomas, S.E., Malek, A., Chen, B., Chen, M., Kim, J., Blundell, T.L., et al. (2018). Arginine-deprivation–induced oxidative damage sterilizes *Mycobacterium tuberculosis*. Proc. Natl. Acad. Sci. USA *115*, 9779–9784. https://doi.org/10.1073/pnas.180887411.

30. Zhao, Z., Wen, S., Song, N., Wang, L., Zhou, Y., Deng, X., Wu, C., Zhang, G., Chen, J., Tian, G.B., et al. (2024). Arginine-enhanced antimicrobial activity of nanozymes against Gram-negative bacteria. Adv. Healthcare Mater. *13*, 2301332. https://doi.org/10.1002/adhm.202301332.

31. Furse, S., and Scott, D.J. (2016). Three-dimensional distribution of phospholipids in Gram-negative bacteria. Biochemist *55*, 4742–4747. https://doi.org/10.1021/acs.biochem.6b00541.

32. Bogdanov, M., Sun, J., Kaback, H.R., and Dowhan, W. (1996). A phospholipid acts as a chaperone in assembly of a membrane transport protein. J. Biol. Chem. *271*, 11615–11618. https://doi.org/10.1074/jbc.271.20.11615.

33. Bogdanov, M., Pyrshev, K., Yesylevskyy, S., Ryabichko, S., Boiko, V., Ivanchenko, P., Kiyamova, R., Guan, Z., Ramseyer, C., and Dowhan, W. (2020). Phospholipid distribution in the cytoplasmic membrane of Gram-negative bacteria is highly asymmetric, dynamic, and cell shape-dependent. Sci. Adv. *6*, eaaz6333. https://doi.org/10.1126/sciadv.aaz6333.

34. Liao, Y., Smyth, G.K., and Shi, W. (2013). The Subread aligner: fast, accurate and scalable read mapping by seed-and-vote. Nucleic Acids Res. *41*, e108. https://doi.org/10.1093/nar/gkt214.

35. Richter, F., Morton, S.U., Qi, H., Kitaygorodsky, A., Wang, J., Homsy, J., DePalma, S., Patel, N., Gelb, B.D., Seidman, J.G., et al. (2020). Whole

genome de novo variant identification with FreeBayes and neural network approaches. Preprint at bioRxiv. https://doi.org/10.1101/2020.03.24.994160.

36. Durrant, M.G., Li, M.M., Siranosian, B.A., Montgomery, S.B., and Bhatt, A.S. (2020). A bioinformatic analysis of integrative mobile genetic elements highlights their role in bacterial adaptation. Cell Host Microbe *27*, 140–153e9. https://doi.org/10.1016/j.chom.2019.10.022.

37. Minh, B.Q., Schmidt, H.A., Chernomor, O., Schrempf, D., Woodhams, M.D., Von Haeseler, A., and Lanfear, R. (2020). IQ-TREE 2: new models and efficient methods for phylogenetic inference in the genomic era. Mol. Biol. Evol. *37*, 1530–1534. https://doi.org/10.1093/molbev/msaa015.

38. Xu, S., Li, L., Luo, X., Chen, M., Tang, W., Zhan, L., Dai, Z., Lam, T.T., Guan, Y., and Yu, G. (2022). Ggtree: a serialized data object for visualization of a phylogenetic tree and annotation data. iMeta *1*, e56. https://doi.org/10.1002/imt2.56.

39. Grabherr, M.G., Haas, B.J., Yassour, M., Levin, J.Z., Thompson, D.A., Amit, I., Adiconis, X., Fan, L., Raychowdhury, R., Zeng, Q., et al. (2011). Full-length transcriptome assembly from RNA-Seq data without a reference genome. Nat. Biotechnol. *29*, 644–652. https://doi.org/10.1038/nbt.1883.

40. Zhao, J., Cheah, S.-E., Roberts, K.D., Nation, R.L., Thompson, P.E., Velkov, T., Du, Z., Johnson, M.D., and Li, J. (2016). Transcriptomic analysis of the activity of a novel polymyxin against *Staphylococcus aureus*. mSphere *1*, e00119-16. https://doi.org/10.1128/mSphere.00119-16.

41. Creek, D.J., Jankevics, A., Burgess, K.E.V., Breitling, R., and Barrett, M.P. (2012). IDEOM: an Excel interface for analysis of LC–MS-based metabolomics data. Bioinform *28*, 1048–1049. https://doi.org/10.1093/bioinformatics/bts069.

42. Kanehisa, M., and Goto, S. (2000). KEGG: Kyoto encyclopedia of genes and genomes. Nucleic Acids Res. *28*, 27–30. https://doi.org/10.1093/nar/28.1.27.

43. Karp, P.D., Billington, R., Caspi, R., Fulcher, C.A., Latendresse, M., Kothari, A., Keseler, I.M., Krummenacker, M., Midford, P.E., Ong, Q., et al. (2019). The BioCyc collection of microbial genomes and metabolic pathways. Briefings Bioinf. *20*, 1085–1093. https://doi.org/10.1093/bib/bbx085.

44. Letunic, I., Yamada, T., Kanehisa, M., and Bork, P. (2008). iPath: interactive exploration of biochemical pathways and networks. Trends Biochem. Sci. *33*, 101–103. https://doi.org/10.1016/j.tibs.2008.01.001.

45. Scheltema, R.A., Jankevics, A., Jansen, R.C., Swertz, M.A., and Breitling, R. (2011). PeakML/mzMatch: a file format, Java library, R library, and tool-chain for mass spectrometry data analysis. Anal. Chem. *83*, 2786–2793. https://doi.org/10.1021/ac2000994.

46. Abraham, M.J., Murtola, T., Schulz, R., Páll, S., Smith, J.C., Hess, B., and Lindahl, E. (2015). GROMACS: High performance molecular simulations through multi-level parallelism from laptops to supercomputers. SoftwareX *1–2*, 19–25. https://doi.org/10.1016/j.softx.2015.06.001.

47. Klauda, J.B., Venable, R.M., Freites, J.A., O'Connor, J.W., Tobias, D.J., Mondragon-Ramirez, C., Vorobyov, I., MacKerell, A.D., Jr., and Pastor, R.W. (2010). Update of the CHARMM all-atom additive force field for lipids: validation on six lipid types. J. Phys. Chem. B *114*, 7830–7843. https://doi.org/10.1021/jp101759q.

48. Lee, J., Patel, D.S., Ståhle, J., Park, S.-J., Kern, N.R., Kim, S., Lee, J., Cheng, X., Valvano, M.A., Holst, O., et al. (2019). CHARMM-GUI membrane builder for complex biological membrane simulations with glycolipids and lipoglycans. J. Chem. Theor. Comput. *15*, 775–786. https://doi.org/10.1021/acs.jctc.8b01066.

49. Zoete, V., Cuendet, M.A., Grosdidier, A., and Michielin, O. (2011). SwissParam: a fast force field generation tool for small organic molecules. J. Comput. Chem. *32*, 2359–2368. https://doi.org/10.1002/jcc.21816.

50. Nelson, A.R.J., and Prescott, S.W. (2019). refnx: neutron and X-ray reflectometry analysis in Python. J. Appl. Crystallogr. *52*, 193–200. https://doi.org/10.1107/S1600576718017296.

51. Weinstein, M.P. (2018). Methods for Dilution Antimicrobial Susceptibility Tests for Bacteria that Grow Aerobically, Eleventh Edition (Clinical and Laboratory Standards Institute).

52. National Health and Medical Research Council (2013). Australian Code for the Care and Use of Animals for Scientific Purposes, Eighth Edition (National Health and Medical Research Council).

53. Roberts, K.D., Zhu, Y., Azad, M.A.K., Han, M.-L., Wang, J., Wang, L., Yu, H.H., Horne, A.S., Pinson, J.-A., Rudd, D., et al. (2022). A synthetic lipopeptide targeting top-priority multidrug-resistant Gram-negative pathogens. Nat. Commun. *13*, 1625. https://doi.org/10.1038/s41467-022-29234-3.

54. Andes, D., and Craig, W.A. (2002). Pharmacodynamics of the new fluoroquinolone gatifloxacin in murine thigh and lung infection models. Antimicrob. Agents Chemother. *46*, 1665–1670. https://doi.org/10.1128/AAC.46.6.1665-1670.2002.

55. Zhu, Y., Zhao, J., Maifiah, M.H.M., Velkov, T., Schreiber, F., and Li, J. (2019). Metabolic responses to polymyxin treatment in *Acinetobacter baumannii* ATCC 19606: integrating transcriptomics and metabolomics with genome-scale metabolic modeling. mSystems *4*, e00157-18. https://doi.org/10.1128/mSystems.00157-18.

56. Han, M.-L., Zhu, Y., Creek, D.J., Lin, Y.-W., Gutu, A.D., Hertzog, P., Purcell, T., Shen, H.-H., Moskowitz, S.M., Velkov, T., and Li, J. (2019). Comparative metabolomics and transcriptomics reveal multiple pathways associated with polymyxin killing in *Pseudomonas aeruginosa*. mSystems *4*, e001499-18. https://doi.org/10.1128/mSystems.00149-18.

57. Joux, F., and Lebaron, P. (2000). Use of fluorescent probes to assess physiological functions of bacteria at single-cell level. Microb. Infect. *2*, 1523–1535. https://doi.org/10.1016/s1286-4579(00)01307-1.

58. Mandavilli, B.S., Aggeler, R.J., and Chambers, K.M. (2018). Tools to measure cell health and cytotoxicity using high content imaging and analysis. Methods Mol. Biol. *1683*, 33–46. https://doi.org/10.1007/978-1-4939-7357-6_3.

59. López-Amorós, R., Castel, S., Comas-Riu, J., and Vives-Rego, J. (1997). Assessment of *E. coli* and *Salmonella* viability and starvation by confocal laser microscopy and flow cytometry using rhodamine 123, DiBAC4 (3), propidium iodide, and CTC. Cytometry *29*, 298–305. https://doi.org/10.1002/(sici)1097-0320(19971201)29:4<298::aid-cyto6>3.0.co;2-6.

60. Deere, D., Porter, J., Edwards, C., and Pickup, R. (1995). Evaluation of the suitability of bis-(1, 3-dibutylbarbituric acid) trimethine oxonol, (diBA-C_4(3)−), for the flow cytometric assessment of bacterial viability. FEMS Microbiol. Lett. *130*, 165–169. https://doi.org/10.1111/j.1574-6968.1995.tb07714.x.

61. Horton, R.M., Cai, Z., Ho, S.M., and Pease, L.R. (2013). Gene splicing by overlap extension: tailor-made genes using the polymerase chain reaction. Biotechniques *54*, 129–133. https://doi.org/10.2144/000114017.

62. Wood, M.W., Jones, M.A., Watson, P.R., Siber, A.M., McCormick, B.A., Hedges, S., Rosqvist, R., Wallis, T.S., and Galyov, E.E. (2000). The secreted effector protein of *Salmonella dublin*, SopA, is translocated into eukaryotic cells and influences the induction of enteritis. Cell Microbiol. *2*, 293–303. https://doi.org/10.1046/j.1462-5822.2000.00054.x.

63. Pelicic, V., Reyrat, J.-M., and Gicquel, B. (1996). Expression of the *Bacillus subtilis sacB* gene confers sucrose sensitivity on mycobacteria. J. Bacteriol. *178*, 1197–1199. https://doi.org/10.1128/jb.178.4.1197-1199.1996.

64. Sun, B., Liu, H., Jiang, Y., Shao, L., Yang, S., and Chen, D. (2020). New mutations involved in colistin resistance in *Acinetobacter baumannii*. mSphere *5*, e00895-19. https://doi.org/10.1128/msphere.00895-19.

65. Fitzsimons, T.C., Lewis, J.M., Wright, A., Kleifeld, O., Schittenhelm, R.B., Powell, D., Harper, M., and Boyce, J.D. (2018). Identification of novel *Acinetobacter baumannii* type VI secretion system antibacterial effector and immunity pairs. Infect. Immun. *86*, e00297-18. https://doi.org/10.1128/IAI.00297-18.

66. Serafimidis, I., Rakatzi, I., Episkopou, V., Gouti, M., and Gavalas, A. (2008). Novel effectors of directed and Ngn3-mediated differentiation of mouse

embryonic stem cells into endocrine pancreas progenitors. Stem Cell. *26*, 3–16. https://doi.org/10.1634/stemcells.2007-0194.

67. Dunstan, R.A., Hay, I.D., and Lithgow, T. (2017). Defining membrane protein localization by isopycnic density gradients. Methods Mol. Biol. *1615*, 81–86. https://doi.org/10.1007/978-1-4939-7033-9_6.
68. Dunstan, R.A., Heinz, E., Wijeyewickrema, L.C., Pike, R.N., Purcell, A.W., Evans, T.J., Praszkier, J., Robins-Browne, R.M., Strugnell, R.A., Korotkov, K.V., and Lithgow, T. (2013). Assembly of the type II secretion system such as found in *Vibrio cholerae* depends on the novel Pilotin AspS. PLoS Pathog. *9*, e1003117. https://doi.org/10.1371/journal.ppat.1003117.
69. Han, M.-L., Zhu, Y., Creek, D.J., Lin, Y.-W., Anderson, D., Shen, H.-H., Tsuji, B., Gutu, A.D., Moskowitz, S.M., Velkov, T., and Li, J. (2018). Alterations of metabolic and lipid profiles in polymyxin-resistant *Pseudomonas aeruginosa*. Antimicrob. Agents Chemother. *62*, e02656-17. https://doi.org/10.1128/AAC.02656-17.
70. Parrinello, M., and Rahman, A. (1981). Polymorphic transitions in single crystals: A new molecular dynamics method. J. Appl. Phys. *52*, 7182–7190. https://doi.org/10.1063/1.328693.
71. Lai, X., Han, M.-L., Ding, Y., Chow, S.H., Le Brun, A.P., Wu, C.-M., Bergen, P.J., Jiang, J.-H., Hsu, H.-Y., Muir, B.W., et al. (2022). A polytherapy based approach to combat antimicrobial resistance using cubosomes. Nat. Commun. *13*, 343. https://doi.org/10.1038/s41467-022-28012-5.
72. Le Brun, A.P., Huang, T.-Y., Pullen, S., Nelson, A.R.J., Spedding, J., and Holt, S.A. (2023). Spatz: the time-of-flight neutron reflectometer with vertical sample geometry at the OPAL research reactor. J. Appl. Crystallogr. *56*, 18–25. https://doi.org/10.1107/S160057672201086X.

STAR★METHODS

KEY RESOURCES TABLE

REAGENT or RESOURCE	SOURCE	IDENTIFIER
Antibiotics		
Colistin sulfate	Sigma	Cat# 4461
Colistin sulfate (test discs)	Oxoid	Cat# 3345446
Spectinomycin	Sigma	Cat# S4014
Tetracycline	Sigma	Cat# T3258
Experimental models: Organisms/strains		
AB5075S	Manoil Laboratory, the University of Washington	N/A
AB5075D	Zhu et al.[16]	N/A
AB5075D transposon insertion mutant library	Manoil Laboratory, the University of Washington	N/A
AB5075D$^{\Delta astA}$	This study	N/A
AB18S	Alfred Hospital, Melbourne, Australia – Prof Denis Spelman (2004)	N/A
AB18D	This study	N/A
AB246S	Women's and Children's Hospital, Adelaide, Australia – Dr Jan Bell and Prof John Turnidge (2006)	N/A
AB246D	This study	N/A
AB3936S	Women's and Children's Hospital, Adelaide, Australia – Dr Jan Bell and Prof John Turnidge (2006)	N/A
AB3936D	This study	N/A
Escherichia coli SM10	Thermo Fisher Scientific	N/A
Pathogen-free Swiss mice	Monash Animal Research Platform, Monash University, Australia	Cat# WDB98086
Chemicals, peptides, and recombinant proteins		
L-arginine	Sigma	Cat# A8094
L-arginine:HCl ($^{13}C_6$, 99%)	Cambridge Isotope Laboratories	Cat# CLM-2265-H
Magnesium sulfate	Chem-supply	Cat# MA048
Sodium chloride	Supelco	Cat# 1.06404.1000
Sodium acetate	Merck	Cat# AM0793268601
Sodium succinate	Sigma	Cat# 2378
Pyruvate	Sigma	Cat# P-2256
Calcium chloride	Sigma	Cat# C4901
Ammonium sulfate	Sigma	Cat# 4418
Ammonium chloride	Sigma	Cat# 9434
Biotin	Sigma	Cat# B4639
L-Amino acids	Sigma	Cat# LAA21-1KT
Spermine	Sigma	Cat# 55513
Spermidine	Sigma	Cat# 49761
Glutathione	Sigma	Cat# G6529
Cyclophosphamide	Baxter	Cat# 8H170D
16:0-18:1 PE (POPE)	Sigma	Cat# 850757P
16:0-18:1 PG (POPG)	Sigma	Cat# 840457P

(*Continued on next page*)

Continued

REAGENT or RESOURCE	SOURCE	IDENTIFIER
18:1 Cardiolipin (TOCL)	Sigma	Cat# 710335P
Bis(1,3-dibutylbarbituric acid) trimethine oxonol (DiBAC)	Sigma	Cat# D8189
CellRox Green	Sigma	Cat# C10444
Pierce BCA protein assay kit	Thermo Fisher Scientific	Cat# 23225
10 x Tris/Glycine/SDS running buffer	Biorad	Cat# 1610732
4–20% Mini-PROTEAN TGX Precast Protein Gels	Biorad	Cat# 4561096
Pre-stained protein standard	Invitrogen	Cat# 57318
Mueller-Hinton broth	Oxoid	Cat# CM0405
Agar	Sigma	Cat# A1296
M9 minimal salts	Sigma	Cat# M6030
DNeasy Blood and Tissue Kit	Qiagen	Cat# 69506
RNeasy Mini Kit	Qiagen	Cat# 74106
Chloroform	Merck	Cat# 102444
Methanol	Merck	Cat# 106035
Deposited data		
DNA and RNA sequencing data	This study	GenBank: PRJNA1084196
Metabolomics and lipidomics data	This study	MetaboLights: MTBLS9708
Oligonucleotides		
qPCR primers, see Table S2	This paper	N/A
Software and algorithms		
GraphPad Prism	GraphStats	https://www.graphpad.com/
Adobe Illustrator	Adobe Inc	https://www.adobe.com/au/products/illustrator.html
SubRead	Liao et al.[34]	https://github.com/ShiLab-Bioinformatics/subread
Freebayes	Richter et al.[35]	https://github.com/freebayes/freebayes
MGEfinder	Durrant et al.[36]	https://github.com/bhattlab/MGEfinder
Roary v3.11.2	GitHub Inc	https://sanger-pathogens.github.io/Roary/
IQ-TREE 2	Minh et al.[37]	http://www.iqtree.org/
ggTree	Xu et al.[38]	https://bioconductor.org/packages/release/bioc/html/ggtree.html
Trinity	Grabherr et al.[39]	https://github.com/trinityrnaseq/
Degust	Zhao et al.[40]	https://degust.erc.monash.edu/
IDEOM	Creek et al.[41]	https://mzmatch.sourceforge.net/ideom.php
MetaboAnalyst 4.0	Chong et al.[20]	https://www.metaboanalyst.ca/
KEGG	Kanehisa et al.[42]	https://www.genome.jp/kegg/
BioCyc	Karp et al.[43]	https://biocyc.org/
iPath 3	Letunic et al.[44]	https://pathways.embl.de/
mzMatch-ISO	Scheltema et al.[45]	https://mzmatch.sourceforge.net/isotopes-targetted.php
Xcalibur Qual Browser	Thermo Fisher Scientific	https://www.thermofisher.com/order/catalog/product/OPTON-30965
NovoExpress software V2.1	ACEA Biosciences, USA	https://www.agilent.com/en/product/research-flow-cytometry/flow-cytometry-software/novocyte-novoexpress-software-1320805
GROMACS 2021	Abraham et al.[46]	https://manual.gromacs.org/2021/index.html
CHARMM36	Klauda et al.[47]	https://www.charmm.org/archive/charmm/resources/charmm-force-fields/

(*Continued on next page*)

Continued

REAGENT or RESOURCE	SOURCE	IDENTIFIER
CHARMM-GUI	Lee et al.[48]	https://www.charmm-gui.org/
Chem3D	The University of Bath	https://library.bath.ac.uk/chemistry-software/chem3d
SwissParam	Zoete et al.[49]	http://www.swissparam.ch/
refnx software	Nelson et al.[50]	https://refnx.readthedocs.io/en/latest/
OmicsNet	Zhou et al.[21]	https://www.omicsnet.ca/
Other		
Illumina HiSeq 2500	Illumnia Inc	https://sapac.support.illumina.com/sequencing/sequencing_instruments/hiseq_2500.html
SeQuant ZIC-pHILIC column	Merck	Cat# 150461
Ascentis Express C8 column	Sigma	Cat# 53831-U
Dionex U3000 high-performance liquid chromatography system	Thermo Fisher Scientific	https://www.thermofisher.com/au/en/home/industrial/chromatography/liquid-chromatography-lc/hplc-uhplc-systems/ultimate-3000-hplc-uhplc-systems.html
Q-Exactive Plus Hybrid Quadrupole-Orbitrap mass spectrometer	Thermo Fisher Scientific	Cat# IQLAAEGAAPFALGMBDK
ACEA NovoCyte high-performance benchtop flow cytometer	ACEA Biosciences, USA	https://www.agilent.com/en/product/research-flow-cytometry/flow-cytometers/flow-cytometer-systems/novocyte-flow-cytometer-systems-1-3-lasers-984681
Tecan Microplate Reader	Tecan	https://lifesciences.tecan.com/multimode-plate-reader
Sorvall WX Ultra Centrifuge	Thermo Scientific	Cat# 75000100
Spatz time-of-flight neutron reflectometer	Australian Nuclear Science and Technology Organisation, Sydney, Australia	https://www.ansto.gov.au/our-facilities/australian-centre-for-neutron-scattering/neutron-scattering-instruments/spatz

RESOURCE AVAILABILITY

Lead contact

Further information and requests for resources and reagents should be directed to and will be fulfilled by the lead contact, Mei-Ling Han (meiling.han@monash.edu).

Materials availability

Bacterial strains and plasmids generated in this study are available upon request to the lead contact.

Data and code availability

- All DNA and RNA sequencing data have been deposited in GenBank (National Library of Medicine, NIH) with accession number GenBank: PRJNA1084196, and all metabolomics and lipidomics data have been deposited in MetaboLights (https://www.ebi.ac.uk/metabolights/) (European Bioinformatic Institutes) with accession number MetaboLights: MTBLS9708.
- All additional information required to reanalyze the data reported in this paper are available from the lead contact upon request.
- This paper does not report original code.

EXPERIMENTAL MODEL AND STUDY PARTICIPANT DETAILS

Bacterial strains and culture

A. baumannii strains AB5075S/D, AB18S/D, AB246S/D and AB3936S/D were grown in Mueller-Hinton (MH) agar (Oxoid, UK) with additional colistin supplementation for polymyxin-resistant strains. To select a polymyxin-dependent mutant, 200 μL of overnight culture was plated on MH agar containing 10 mg/L colistin. The resulting colonies were then resuspended in saline and plated on MH agar upon which was placed a sterile paper disc containing 10 μg colistin. Colonies that grew around the disc but not elsewhere on the plate were selected as polymyxin-dependent mutants. These polymyxin-dependent strains including AB5075D exhibited defective growth on MH agar in the absence of colistin, with growth significantly improved by the supplementation with 10 mg/L colistin (Figure S1A). Similarly, poor growth of these strains in colistin-free MH broth was also significantly improved with colistin supplementation (1–128 mg/L) (Figure S1B). Transposon insertion mutants of AB5075 were purchased from the Manoil Laboratory at the University of Washington. *Escherichia coli* SM10 (Thermo Fisher Scientific, Waltham, MA) was cultured in Luria-Bertani broth with

appropriate antibiotic supplementation. Colistin MICs were measured using broth microdilution according to the Clinical and Laboratory Standards Institute standards.[51]

METHOD DETAILS

Metabolite supplementation

Major amino acids (including L-arginine, lysine, alanine, aspartate, glycine, ornithine, proline, glutamate, glutamine, serine, cystine, and histidine), carbon sources (including sodium acetate, sodium succinate, and pyruvate), and nitrogen sources (including ammonium chloride and ammonium sulfate) all at 10 mM, biotin at 1 mM, and polyamines (including spermine and spermidine) and glutathione at 0.1 mM were separately added to MH agar media, with non-supplemented MH agar as the control. Bacterial suspensions were prepared for individual polymyxin-dependent strains AB5075D, AB18D, AB246D, and AB3936D (MacFarland standard at 1.0 ± 0.1) and diluted 1:10 in sterile saline. Each bacterial suspension at a volume of 100 μL was manually spread onto one-quarter of the above supplemented or non-supplemented agar plates. A sterile paper disc containing 10 μg colistin was placed at the center of each plate (which contained all four strains in separate quarters) to visualize polymyxin dependence for each strain. All agar plates were incubated overnight at 37°C.

Neutropenic murine thigh infection model

The animal experiment was approved by Monash Animal Ethics Committee (approval ID: 13447) and the animals maintained in accordance with the Australian Code of Practice for the Care and Use of Animals for Scientific Purpose.[52] The neutropenic mouse thigh infection model was undertaken over 18 h, as described previously.[53] Briefly, pathogen-free Swiss mice (female, 8-week-old, 24–30 g) were rendered neutropenic by intraperitoneal administration of cyclophosphamide 4 days (150 mg/kg) and 1 day (100 mg/kg) prior to bacterial inoculation. Thigh infection with AB18S/D (polymyxin-susceptible, S; polymyxin-dependent, D), AB246S/D, and AB3936S/D was established via administration of early log-phase bacterial suspension ($\sim 10^5$ CFU bacteria; injection volume, 50 μL; four thighs from two mice per group)[54]; an equivalent volume of sterile saline was administered to the control group. Two hours after inoculation (considered 0 h), colistin sulfate (30 mg/kg) was injected subcutaneously 6-hourly for 18 h. At 0 and 18 h after colistin treatment, 2 mice from each group (including both polymyxin-susceptible and -dependent strains with or without colistin) were euthanized and each thigh collected, homogenized, and filtered under sterile conditions. Appropriately diluted (in sterile saline) homogenate was spread on nutrient agar plates containing 0, 2, or 16 mg/L colistin and the bacterial load in both thighs ($\log_{10}$ CFU/thigh) for each mouse determined.

Whole genome sequencing

The genomic DNA of the aforementioned polymyxin-dependent strains was extracted using a DNeasy Blood and Tissue Kit and sequenced using Illumina HiSeq 2500 (Genewiz, Suzhou, China). Raw reads were trimmed and aligned using Subread,[34] single-nucleotide polymorphisms (SNPs) were analyzed using freebayes,[35] while indels and insertion sequences were identified using MGEfinder.[36] Core-SNP alignments were detected by comparing all 15,049 genomes using Roary v3.11.2 (https://sanger-pathogens.github.io/Roary/). A phylogenetic tree was constructed based on the core-SNP alignment with a GTR model and ascertainment bias correction using IQ-TREE 2,[37] and then visualized using ggtree v3.6.2.[38]

Comparative transcriptomics and metabolomics

Bacterial colonies of both polymyxin-susceptible and -dependent strains were resuspended in sterile saline and adjusted to a MacFarland standard of 1.0–1.2. Each culture was then diluted 1:20 with fresh cation-adjusted MHB (CAMHB) and grown to early log phase ($\sim 10^8$ CFU/mL; optical density at 600 nm [OD_{600}], ~0.50). Polymyxin-dependent strains were then treated with 16 mg/L colistin for 2 h, with an untreated culture as the control. Total RNA from each sample was extracted using an RNeasy Mini Kit (Qiagen) and sequenced using Illumina HiSeq. RNA sequencing data were analyzed as previously reported.[40,55] Briefly, the transcriptome was assembled using Trinity,[39] and the reads were aligned using Subread.[34] The statistical analysis was conducted in Degust based on Voom and Limma linear models.[40]

Metabolomics was undertaken as described previously, with bacterial whole cell metabolites extracted using chloroform/methanol/water (CMW, 1:3:1, v/v) containing 1 μM generic internal standards (CHAPS, CAPS, PIPES and TRIS), and analyzed by hydrophilic interaction liquid chromatography (HILIC).[56] Pooled quality control samples were included to evaluate analyte stability, and a mixture of approximately 400 authentic metabolite standards was analyzed to assist in metabolite identification. The IDEOM software was applied for metabolite identification and quantification,[41] and MetaboAnalyst 4.0 was employed for univariate (e.g., one-way ANOVA) and multivariate (e.g., PCA) statistical analysis.[20] Integrative transcriptomic and metabolomic pathway analysis was conducted based on the KEGG[42] and BioCyc[43] databases and visualized in iPath 3.[44]

Stable isotope labeling

Polymyxin-susceptible AB5075S and polymyxin-dependent AB5075D were streaked onto Mueller-Hinton agar, in the absence or presence of 16 mg/L colistin, respectively, and grown overnight at 37°C. Single colonies were then selected and resuspended in 3 mL of sterile saline (~1.0 MacFarland standard) and diluted 1:20 in 57 mL of M9 minimal media (Cat# M6030, Sigma-Aldrich),

with 5 mM arginine as the sole carbon source. Bacterial cultures were then incubated at 37°C (shaking speed of 150 rpm) for ~4 h to reach early log phase growth (OD_{600} ~0.3). The media was then removed via centrifugation at 4,000 × *g* for 15 min at room temperature and replaced with the same volume of M9 media containing 5 mM $^{13}C_6$-L-arginine (99%; CLM-2265-H; Cambridge Isotope Laboratories, Inc.) as the sole carbon source. Bacterial samples (5 mL) were collected at 0, 15, 30, 60, and 120 min and pelleted by centrifugation (4,000 × *g* for 15 min). Whole cell metabolites were extracted using chloroform/methanol/water (CMW, 1:3:1, v/v) and analyzed by the HILIC method.[56] Isotope labeling was performed with mzMatch-ISO software,[45] with all putative metabolites identified in the above comparative metabolomics serving as a metabolite library to extract all isotopologue peaks. To correct the results for those isometric metabolites that may overlap in this large-scale automated process, additional analysis of metabolite labeling was performed in Xcalibur Qual Browser (Thermo).

Flow cytometry analysis

Intracellular oxidative stress and the membrane integrity of the polymyxin-susceptible and -dependent strains of *A. baumannii* was investigated using an ACEA NovoCyte high-performance benchtop flow cytometer (ACEA Biosciences, Santa Clara, CA, USA).[57] CellROX-Green (CR-G) (Sigma-Aldrich, Castle Hill, NSW, Australia, Ex/Em 488/660–690 nm) was used to measure intracellular oxidative stress,[58] and the voltage-sensitive fluorophore Bis-(1,3-Dibutylbarbituric Acid) Trimethine Oxonol (DiBAC) (Sigma-Aldrich, Castle Hill, NSW, Australia, Ex/Em 488/660–690) was used as a marker of bacterial membrane depolarization.[59,60] All samples were analyzed using the blue laser detection channel pre-set with a threshold forward scatter (FSC-H) and side-scatter (SSC-H) of >1,000 units, events per second <1,000, and a maximum acquisition of 20,000 events. Paired wild-type and polymyxin-dependent strains were exposed to colistin (1 mg/L for polymyxin-susceptible strains and 16 mg/L for -dependent strains), 10 mM arginine, or their combination. Bacterial samples (0.4 mL) were collected at 30 and 90 min, pelleted (14,000 × *g* for 5 min at 4°C), and resuspended in 0.2 mL of sterile saline. The bacterial samples were appropriately diluted and separately stained with 2.5 μM CR-G or 6 μM DiBAC and incubated for 45 min and 2 min, respectively. Excess dye was removed through centrifugation (14,000 × *g* for 5 min at 4°C) prior to analysis. Fluorescence intensity data were analyzed and log-transformed using the NovoExpress software V2.1 (ACEA Biosciences, USA).

Construction of *astA* deletion and complementation in AB5075D

The splicing Overlap Extension (SOEing) reaction was used to generate disrupted fragment, *astA:TcR:FRT*, which contains a tetracycline resistance marker flanked by 1 kb upstream and 1 kb downstream homologous DNA sequences of the *astA* gene.[61] The *astA:TcR:FRT* fragment was gel purified and cloned into a linear pDM4 suicide plasmid digested with SmaI.[62] The disruption of *astA* in AB5075D was carried out by biparental conjugation using *E. coli* SM10 donor cells carrying the suicide vector pDM4 ligated to the *astA:TcR:FRT* fragment. Colonies were patched onto LB agar plates containing 1 mg/L tetracycline and 50 mg/L spectinomycin to eliminate the growth of *E. coli* SM10. Patched colonies were then selected for a second recombination using the *sacB* gene located on the backbone of pDM4 and grown on LB plates containing 15% sucrose.[63] Single colonies were then patched onto LB plates containing 1 mg/L tetracycline, and *astA:TcR:FRT* gene disruption in AB5075D confirmed by PCR. To make a clean deletion of *astA*, the pAT03-Apr plasmid was employed to excise the tetracycline resistance cassette by the expression of FLP recombinase.[64] The *astA* deletion mutant of AB5075D was verified by PCR and whole genome sequencing. For the complementation of *astA* into AB5075D, the shuttle vector pBASE was originally constructed by Fitzsimons et al.,[65] and the *bla* cassette (861 bp) was removed by double digestion using AatII and NotI restriction enzymes. Primers with AatII and NotI restriction sites were designed for the amplification of *apmR* (801 bp) from the pAT03-Apr plasmid, which encodes an aminoglycoside 3-*N*-acetyltransferase. The PCR product was gel purified, then double digested by NotI and AatII, and cloned into pBASE backbone. The full-length *astA* gene was amplified using forward and reverse primers containing AatII and KpnI restriction sites. The purified PCR product was then ligated into pBASE-AprR, digested with AstII and KpnI, and transformed into AB5075D$^{\Delta astA}$.[66] The complemented mutant harboring the pBASE-AprR-*astA* plasmid was confirmed by PCR. All primers used in this study are listed in Table S2.

Membrane lipidomics and lipid A profiling

Bacterial strains AB5075S, AB5075D, and the *astA* deletion mutant AB5075D$^{\Delta astA}$ were grown in 400 mL of CAMHB until reaching an OD_{600nm} of 0.8–1.0. Bacterial cell pellets were collected via centrifugation (8,000 × *g* for 15 min at 4°C) and resuspended in 0.75 M sucrose/10 mM Tris-HCl, pH 7.5. This was followed by the sequential addition of 50 μg/mL lysozyme, 2 mM PMSF, and 2 volumes of 1.65 M EDTA (pH 7.5), and homogenization with an EmulsiFlex cell disruptor (Avestin Inc.).[67] Total membranes were collected by ultracentrifugation (132,000 × *g* for 45 min at 4°C) and fractionated by a six-step sucrose gradient (35%:40%:45%:50%:55%:60%, w/v, sucrose in 5 mM EDTA, pH 7.5) through ultracentrifugation (205,000 × *g* for 17 h at 4°C). Each outer and inner membrane sample was normalized based on a bicinchoninic acid (BCA) assay.[17,67,68] The membrane lipids were extracted with a double-phase Bligh-Dyer solution (chloroform/methanol/water, 1:1:0.9, v/v), and the lipid A samples were prepared using a mild-acid hydrolysis method.[69] All membrane lipid samples were analyzed by reversed-phase LC-MS/MS through a Dionex Ultimate 3000 high-performance liquid chromatography coupled with a Q-Exactive Orbitrap mass spectrometer (Thermo Fisher Scientific, USA). To assist in membrane lipid identification, 10 μL of each lipid sample was mixed together and concentrated 10-fold to generate a lipid library based on the MS/MS spectrum. Commercial phospholipid standards (including PE 17:0/14:1, PG 17:0/14:1, and CL $(15:0)_3$-16:1; Avanti Polar Lipids) at 0.1,

0.25, 0.5, 1.0, 2.5, and 5.0 μM were also analyzed within the same batch to assist in the quantification of major membrane phospholipids.

Molecular dynamic simulations

The all-atom MD simulations were conducted using GROMACS 2021[46] with the CHARMM36 all-atom force field.[47] Based on our membrane lipidomics data (Figure 6D), the OM models for both Ab5075D and AB5075D$^{\Delta astA}$ were constructed using the CHARMM-GUI membrane builder.[48] A total of 4 membrane systems were constructed: i) AB5075D OM only; ii) AB5075D OM with colistin; iii) AB5075D$^{\Delta astA}$ OM only; and iv) AB5075D$^{\Delta astA}$ OM with colistin. For each membrane system, four colistin A molecules with the topology generated by Chem3D and SwissParam server[49] were placed above the membrane surface at random positions. In the simulation, energy minimization was first performed to alleviate inappropriate contacts, followed by six equilibrations during which the position restraints on the lipids in the NPT ensemble were gradually turned off. The production run was performed for 100 ns with the temperature maintained at 310 K using the Nose-hoover algorithm and the pressure maintained at 1 bar using Parrinello-Rahman barostat.[70] MD parameters are listed in Table S4.

Neutron reflectometry measurement and data analysis

The LPS-deficient outer membrane bilayers of AB5075D (containing 36.3% 16:0-18:1 PE (POPE), 44.8% 16:0-18:1 PG (POPG), and 18.9% (18:1)$_3$-cardiolipin (TOCL)) and its *astA* deletion mutant AB5075D$^{\Delta astA}$ (containing 64.9% POPE, 23.0% POPG, and 12.1% TOCL) were prepared on 100-mm diameter round silicon wafers using the Langmuir-Blodgett and Langmuir-Schaefer techniques based on our membrane lipidomics results.[25,71] The assembled outer membrane bilayers contained within aluminum solid-liquid cells were measured using the Spatz time-of-flight neutron reflectometer at the 20MW OPAL Reactor at the Australian Nuclear Science and Technology Organisation (ANSTO), Sydney, Australia.[72] A cold neutron spectrum (2.8 Å $\leq \lambda \leq$ 18 Å) and a chopper pairing of choppers 1 and 2 with a separation of 480 mm set to 25 Hz rotation speed were used to provide a wavelength resolution ($\Delta\lambda/\lambda$) at −5%. To cover the momentum transfer (Q) ranging from 0.01 to 0.3 Å^{-1}, the neutron beams reflected from the sample interface were collected at two glancing angles (0.85° and 3.5°) of incidence using a 55-mm footprint and $\Delta\theta/\theta$ of 3%. Here, the momentum transfer Q is defined as: $Q = 4\pi \sin(\theta)/\lambda$, where θ is the angle of incidence and λ is the wavelength. To characterize the outer membrane bilayers and their interaction with colistin, a total of three contrasts with scattering length density (SLD, ρ) was used, namely D_2O (ρ = 6.35 × 10^{-6} Å^{-2}), CMSi (contrast-matched silicon, 38% D_2O/62% H_2O, ρ = 2.07 × 10^{-6} Å^{-2}), and H_2O (ρ = −0.56 × 10^{-6} Å^{-2}). Between each contrast, 10 mL of buffer solution (10 mM HEPES, 5 mM $CaCl_2$, and 150 mM NaCl; pH 7.4) was pumped through the sample wafer at a rate of 1.0 mL/min using an HPLC pump (Knauer GmbH, Berlin, Germany). Following the successful characterization of the membrane bilayer, 4 mL of colistin at 16 or 128 mg/L was subsequently injected into the bilayer and incubated for 2 h. Each treatment was measured using all three contrasts as mentioned above.

The neutron reflectometry data were firstly reduced using the reduction routine within the refnx software to provide a complete reflectivity profile and scaled to ensure the critical edge equaled one.[50] Data analysis of neutron reflectometry profiles was performed using the refnx analysis program, with final fitting carried out using the Markov Chain Monte Carlo (MCMC) simulation method for error analysis.[50] For data fitting, parameters including thickness, SLD (Table S7), and roughness were used to define each sublayer of the outer membrane bilayer, with parameters varied until the lowest χ^2 value was achieved. The reflectometry profiles of the bilayer under all three different contrasts (D_2O, CMSi, and H_2O) were fitted simultaneously to determine the volume fraction of solvent (φ_{water}) binding to each sublayer. The volume fraction of phospholipids (φ_{layer}) within each sublayer or colistin at the surface of the bilayer was then determined ($\varphi_{layer} = 1\text{-}\varphi_{water}$).

QUANTIFICATION AND STATISTICAL ANALYSIS

All figures were generated in Adobe Illustrator (Version 24.1) and GraphPad Prism (Version 10.0, GraphPad Software). Univariate and multivariate statistical analyses for transcriptomics and metabolomics data were performed with Degust (https://degust.erc.monash.edu/) and MetaboAnalyst 4.0,[20] respectively. Differentially expressed genes (DEGs) were determined using Degust based on Voom and Lima linear models,[40] while differentially changed metabolites (DCMs) were identified based on one-way ANOVA with a post-hoc test. Data displayed in bar charts are represented as means ± SD, with the statistical analyses (unpaired *t* test, one-way or two-way ANOVA with Tukey's correction) performed using GraphPad Prism. A p value of less than 0.05 was considered statistically significant.